Journal of Cosmology and Astroparticle Physics
An IOP and SISSA journal

Received: *March 27, 2024*
Revised: *December 9, 2024*
Accepted: *December 12, 2024*
Published: *January 14, 2025*

Minimal decaying dark matter: from cosmological tensions to neutrino signatures

Lea Fuß, Mathias Garny and Alejandro Ibarra

TUM School of Natural Sciences, Department of Physics, Technical University of Munich, James-Franck-Str. 1, 85748 Garching, Germany

E-mail: lea.fuss@tum.de, mathias.garny@tum.de, alejandro.ibarra@tum.de

Abstract: The invisible decay of cold dark matter into a slightly lighter dark sector particle on cosmological time-scales has been proposed as a solution to the S_8 tension. In this work we discuss the possible embedding of this scenario within a particle physics framework, and we investigate its phenomenology. We identify a minimal dark matter decay setup that addresses the S_8 tension, while avoiding the stringent constraints from indirect dark matter searches. In our scenario, the dark sector contains two singlet fermions $N_{1,2}$, quasi-degenerate in mass, and carrying lepton number so that the heaviest state (N_2) decays into the lightest (N_1) and two neutrinos via a higher-dimensional operator $N_2 \to \bar{N}_1 \nu\nu$. The conservation of lepton number, and the small phase-space available for the decay, forbids the decay channels into hadrons and strongly suppresses the decays into photons or charged leptons. We derive complementary constraints on the model parameters from neutrino detectors, freeze-in dark matter production via $\nu\nu \to N_1 N_2$, collider experiments and blazar observations, and we show that the upcoming JUNO neutrino observatory could detect signals of dark matter decay for model parameters addressing the S_8 tension if the dark matter mass is below $\simeq 1\,\mathrm{GeV}$.

Keywords: dark matter theory, particle physics - cosmology connection

ArXiv ePrint: 2403.15543

https://doi.org/10.1088/1475-7516/2025/01/055

JCAP01(2025)055

Contents

JCAP01(2025)055

1 Introduction

The ΛCDM model describes with remarkable accuracy numerous cosmological observations, including the anistropies in the cosmic microwave background (CMB) and the large-scale structure (LSS) of our Universe. On the other hand, a few observations seem to be in tension with the ΛCDM model and may indicate the necessity of an extension. The most conspicuous tension is the discrepancy between the values of the Hubble constant inferred from early and late Universe observables; this is the well known Hubble tension (see for example [1]). Furthermore, a tension between the amplitudes of density perturbations inferred from primary CMB or from LSS probes has been reported. This is the so-called S_8 tension, where $S_8 = \sigma_8 \sqrt{\Omega_m/0.3}$ (here, σ_8 describes the matter fluctuations at scales of $8\,\mathrm{Mpc}/h$ and Ω_m is the matter density parameter).

More specifically, various LSS measurements, including e.g. weak lensing shear, galaxy clustering and cluster number counts have reported lower values compared to the one derived from Planck CMB data with $S_8 = 0.830 \pm 0.013$ [2]. While the significance for each data set is typically only at the level of $1 - 3\sigma$, they all seem to show a common trend [3, 4]. The strongest deviation was found from weak lensing by the Kilo-Degree Survey KiDS-1000 [5]

with $S_8 = 0.759^{+0.024}_{-0.021}$, while the Dark Energy Survey (DES) reports $S_8 = 0.776^{+0.017}_{-0.017}$ [6], and an updated combined analysis of the two obtained $S_8 = 0.790^{+0.018}_{-0.014}$ [7] (for measurements sensitive to larger scales see for example [8–10]). Despite efforts to explain the S_8 tension with baryonic or systematic effects it is not easily resolved [11, 12]. Another strategy to address the tension is to go beyond ΛCDM by changing the dark sector to achieve a suppression of dark matter (DM) clustering, see e.g. [3]. Even though some models are able to lower the S_8 value and thus decrease the tension, there is no definite preference over ΛCDM for any of them yet. New surveys, like Euclid [13], DESI [14] and the LSST survey at the Vera C. Rubin observatory [15], will probe the amplitude of density perturbations on a wide range of scales and redshifts, and may elucidate in the near feature whether the S_8 tension is real.

A promising scenario that addresses the S_8 tension is decaying cold dark matter (DCDM). In this scenario, a cold dark matter (CDM) particle decays into invisible final states on cosmological time-scales. The cosmological signatures have been studied extensively for massless secondaries [16–25] as well as for massive ones [26–42], including probes from the CMB as well as large- and small-scale structure like baryon acoustic oscillations, galaxy clustering, weak lensing, the Lyman-α forest and Milky Way satellites. Here we focus on a scenario in which the CDM particle is quasi-degenerate in mass with one of the daughter particles in the decay, but with a mass difference that allows the other decay products to be relativistic, being one of the setups that has received increased attention in the context of the S_8 tension lately [26–42]. In this scenario, there is a conversion of the rest energy of the mother particle into kinetic energy of the heaviest massive daughter, which gradually builds up a population of warm dark matter (WDM) particles coexisting with the population of CDM particles. This leads to a mild suppression of the matter power spectrum on small scales and at late times. The amount and scale of power suppression depend on the lifetime τ as well as the available fraction of kinetic energy ϵ, respectively. Typical values for alleviating the S_8 tension are $\tau \simeq \mathcal{O}(10 - 100)\,\mathrm{Gyrs}$ and $\epsilon \simeq 10^{-2} - 10^{-3}$ [36, 37, 39, 40, 42].

In this work, we identify a minimal embedding of the DCDM scenario within a particle physics framework (see [43–50] for related works). We first discuss the necessary elements of a DCDM scenario which addresses the S_8 tension while complying naturally with the stringent limits from gamma-ray and cosmic-ray observations. We then construct a gauge-invariant and Lorentz-invariant operator leading to DCDM, show that it is the simplest one under certain assumptions, and discuss the associated phenomenology in the Early Universe, as well as the possible signatures in laboratory experiments or in astrophysical observations.

The paper is structured as follows: In section 2, we give a brief overview of DCDM and its existing phenomenology and cosmological signatures. Then, the concrete minimal model is developed and motivated in section 3, including an evaluation of the main decay channel. Next, in section 4 we derive limits from diffuse neutrino flux measurements. In section 5 we consider freeze-in production of DM within the minimal model. In section 6 we discuss complementary signatures, including higher-order decays into charged particles and gamma-rays, invisible Higgs decay, as well as neutrino flux attenuation from blazars due to neutrino-DM scatterings. We conclude in section 7. The appendices provide further technical material, relevant for the computation of decay rates, for freeze-in, neutrino-DM scattering, as well as a discussion of the limit of very low DM masses.

JCAP01(2025)055

2 The decaying cold dark matter scenario and the S_8 tension

The simplest DCDM scenario addressing the S_8 tension consists of a population of initially cold dark matter (DCDM) decaying into one massive and one massless particle species, that act as warm dark matter (WDM) and dark radiation (DR), respectively [36, 37, 39, 40, 42]

$$\text{DCDM} \;\rightarrow\; \text{WDM} \;+\; \text{DR}\,. \tag{2.1}$$

From the point of view of cosmology all "dark" particle species are assumed to have negligible interactions with visible matter at the relevant time-scales, i.e. during and after the recombination epoch. We note that the Standard Model (SM) neutrinos satisfy all the requirements to be "dark radiation" with this definition, as we will emphasize below.

The effects of DCDM on cosmology can be entirely captured by two parameters: the decay rate Γ (or equivalently the lifetime $\tau = \Gamma^{-1}$), and the relative mass splitting ϵ, defined as

$$\epsilon \equiv \frac{1}{2}\left(1 - \frac{m^2}{M^2}\right)\,, \tag{2.2}$$

where M and m are the masses of the DCDM and the WDM particles, which determines the fraction of rest mass that is converted into kinetic energy in the decay. In this paper, we focus on the limit when the DCDM and the WDM particles are quasi-degenerate in mass, namely $\epsilon \ll 1$, so that there is a gradual "heating" of the DM as more and more CDM particles decay, and that is investigated in view of the S_8 tension [26–42].

The Boltzmann equations for this setup include source and loss terms for the respective new dark species. At the homogeneous and isotropic background level, they are given by [36]

$$\begin{aligned}
\dot{\bar{f}}_{\rm dcdm}(q,\tau) &= -a\Gamma \bar{f}_{\rm dcdm}(q,\tau)\,,\\
\dot{\bar{f}}_{\rm wdm}(q,\tau) = \dot{\bar{f}}_{\rm dr}(q,\tau) &= \frac{a\Gamma \bar{N}_{\rm dcdm}}{4\pi q^2}\delta(q - a p_{\text{2-body}})\,,
\end{aligned} \tag{2.3}$$

where f are the respective phase-space distribution functions, $q = ap$ is the co-moving momentum, a the scale-factor and $\bar{N}_{\rm dcdm}$ the number density of the mother particle, which drops exponentially in time. A dot denotes derivative with respect to conformal time η, related to the usual cosmic time t via $d\eta = dt/a$. Multiplying the Boltzmann equations with the respective particle energies and integrating over all momentum modes yields equations for the average energy densities denoted by $\bar{\rho}$,

$$\begin{aligned}
\dot{\bar{\rho}}_{\rm dcdm} &= -3\mathcal{H}\bar{\rho}_{\rm dcdm} - a\Gamma\bar{\rho}_{\rm dcdm}\,,\\
\dot{\bar{\rho}}_{\rm dr} &= -4\mathcal{H}\bar{\rho}_{\rm dr} + \epsilon a\Gamma\bar{\rho}_{\rm dcdm}\,,\\
\dot{\bar{\rho}}_{\rm wdm} &= -3(1+\omega)\mathcal{H}\bar{\rho}_{\rm wdm} + (1-\epsilon)a\Gamma\bar{\rho}_{\rm dcdm}\,,
\end{aligned} \tag{2.4}$$

with $\mathcal{H} = aH$ where H is the Hubble rate, and with the equation-of-state parameter $\omega = \bar{P}_{\rm wdm}/\bar{\rho}_{\rm wdm}$ for WDM where $\bar{P}_{\rm wdm}$ is the average pressure. On top of the usual cosmological evolution, the terms involving Γ describe the impact of the decay on the background densities.

JCAP01(2025)055

The phenomenology of this scenario has been discussed in various works, e.g. [26, 36, 39, 40, 42, 51]. The most prominent implication is a suppression of the matter power spectrum on small scales, being linked to the S_8 tension. Since the massive decay product receives a velocity kick, part of the DM develops a non-zero pressure and acts like a warm DM component building up over time. Compared to CDM, the additional WDM can more easily escape overdensities and wash out structure on small physical scales. This leads to a gradual suppression of the power spectrum for large wavenumbers k. Since ϵ determines the momentum of the WDM, it sets the free-streaming scale and thus the wavenumber at which the suppression starts. In contrast, the decay time τ controls the fraction of WDM at any given redshift z and is responsible for the amount of suppression. Notably, the decay implies a pronounced redshift-dependence of the amplitude of suppression.

Another related effect of the velocity kick is the difference in halo evolution compared to CDM. For small enough halos, with typical virial velocities of the order of or below the kick velocity, WDM particles are able to disrupt or escape the halo. This suppresses the number of small halos compared to the ΛCDM model [26, 51]. Apart from matter fluctuations, DCDM can change the cosmological background evolution as described in eq. (2.3). However, this effect is negligible for sufficiently large τ or small ϵ. For $10^5\,\mathrm{yr} \ll \tau \ll t_0$ and sizeable ϵ, the extra DR increases the distance to the sound horizon which then requires a higher Ω_Λ (and thus H_0) to not shift the acoustic peaks in the CMB anisotropy spectrum. While this possibility has been discussed in context of the Hubble tension, it is highly constrained by supernova, baryonic acoustic oscillation (BAO) and CMB data [39, 52].

Overall, DCDM with $\tau \gtrsim t_0$ and $\epsilon \ll 1$ can primarily be probed by LSS data as well as halo abundances and properties. In figure 1, we show a collection of cosmological constraints on DCDM in the $\epsilon - \tau$ plane, where the upper left corner converges to ΛCDM. In blue, limits from combining Planck CMB, BAO and Pantheon supernova data as obtained in [39] are shown. Note that this result was actually reported as a confidence interval around the best fit value, that we inverted to indicate which values are approximately excluded. In pink, we show limits from [40], where the Lyman-α flux power spectrum measured by BOSS at $z = 3.0 - 4.2$ [53] was used to constrain the matter power spectrum. In gray, we display results from a weak lensing shear analysis performed in [42], leading to rather strong constraints. In this work, an emulator was trained to determine the power spectrum of DCDM on non-linear scales, including baryonic effects, in order to analyze KiDS-1000 [5] combined with Planck CMB data [2]. Similar to the CMB constraints, we emphasize that the original work determined confidence intervals that we inverted to map out an approximate exclusion region. Since the analysis was only done up to $\epsilon = 10^{-2}$, the bound stops abruptly at this point and it is not entirely clear how it could be extrapolated. However, even if we assume a straight continuation of the exclusion line, our conclusions would not change significantly. Finally, in olive we show constraints from [26] derived from Milky Way satellite abundances and the respective halo mass functions for two different velocity kicks that are then extrapolated to higher values.

For illustration, the dark red contour lines in figure 1 show the (ϵ, τ) parameters for which DCDM can reproduce the S_8 values reported by KiDS, $S_8 = 0.759$ [5], and KiDS+DES,

JCAP01(2025)055

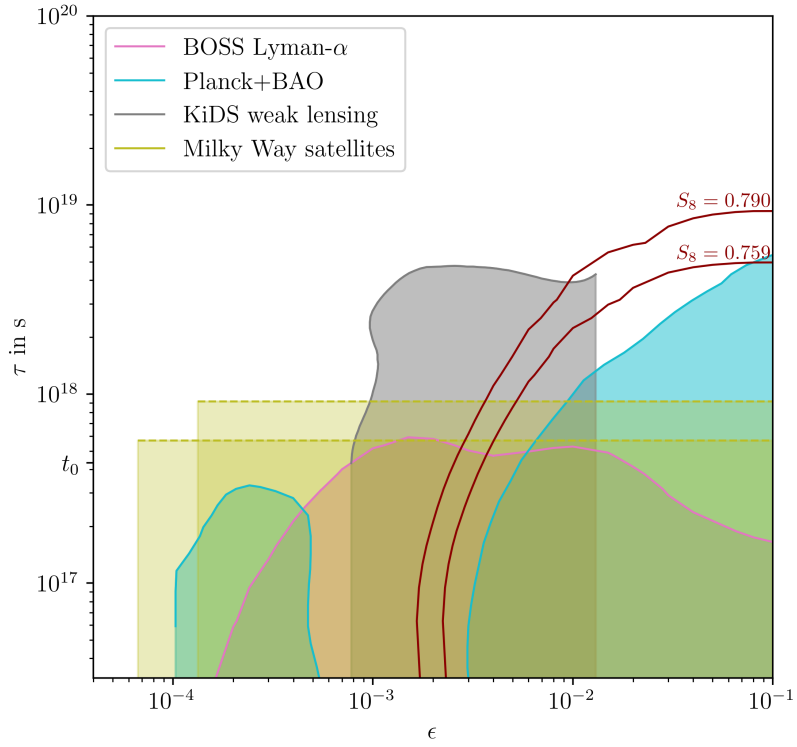

Figure 1. Allowed parameter space of the decaying cold dark matter scenario DCDM $\rightarrow$ WDM + DR. The region between the two thick red lines highlights the region in parameter space addressing the S_8 tension, and the shaded regions show various constraints derived from Lyman-α, CMB, weak lensing and Milky Way satellite data (see legend and main text for details). On the y-axis, t_0 indicates the age of the Universe.

$S_8 = 0.79$ [7], respectively. All other cosmological model parameters are set to the Planck 2018 best-fit values [2] within ΛCDM to obtain the contour lines, motivated by the fact that DCDM and ΛCDM are indistinguishable at times $t \ll \tau$, i.e. in particular around recombination. For comparison, within ΛCDM $S_8 = 0.83$ for Planck parameters. As can be seen in figure 1, current cosmological constraints on DCDM still leave an open window where the S_8 value can be reduced. Typical values in this window are of the order of $\epsilon \simeq 0.01$ and $\tau \simeq 100\,\mathrm{Gyrs} \simeq 3 \cdot 10^{18}\,\mathrm{s}$.

This simple setup can be extended to include more DR particles in the final state, for instance the three-body DCDM decay [30, 40]

$$\mathrm{DCDM} \rightarrow \mathrm{WDM} + \mathrm{DR}_a + \mathrm{DR}_b\,. \tag{2.5}$$

As for the two-body decays, the cosmological implications of the decay can be encoded in the decay rate, Γ, and in the fraction of the energy of the mother particle that is converted into kinetic energy, determined by the mass splitting ϵ in eq. (2.2). On the other hand, this scenario presents the complication that the decay products have a continuous momentum distribution, $d\Gamma/dq_i$, with q_i the momenta of the different daughter particles, and which is

JCAP01(2025)055

highly model dependent. The Boltzmann equations at the background level then read [40]

$$\begin{aligned}\dot{\bar{f}}_{\rm dcdm}(q,\tau) &= -a\Gamma \bar{f}_{\rm dcdm}(q,\tau)\,,\\ \dot{\bar{f}}_{\rm wdm}(q_1,\tau) &= \frac{a\Gamma \bar{N}_{\rm dcdm}}{4\pi q_1^2}\left(\frac{1}{\Gamma}\frac{d\Gamma}{dq_1}\right)\,,\\ \dot{\bar{f}}_{{\rm dr}_{a,b}}(q_{2,3},\tau) &= \frac{a\Gamma \bar{N}_{\rm dcdm}}{4\pi q_{2,3}^2}\left(\frac{1}{\Gamma}\frac{d\Gamma}{dq_{2,3}}\right)\,.\end{aligned} \tag{2.6}$$

Compared to eq. (2.3) the Dirac delta is replaced by the momentum distribution. Multiplying these equations by energy and integrating over momentum yields evolution equations for the energy density, thus generalizing eq. (2.4) to three-body decays

$$\begin{aligned}\dot{\bar{\rho}}_{\rm dcdm} &= -3\mathcal{H}\bar{\rho}_{\rm dcdm} - a\Gamma\bar{\rho}_{\rm dcdm}\,,\\ \dot{\bar{\rho}}_{\rm dr} &= -4\mathcal{H}\bar{\rho}_{\rm dr} + (2\langle E_{\rm dr}\rangle/M)a\Gamma\bar{\rho}_{\rm dcdm}\,,\\ \dot{\bar{\rho}}_{\rm wdm} &= -3(1+\omega)\mathcal{H}\bar{\rho}_{\rm wdm} + (\langle E_{\rm wdm}\rangle/M)a\Gamma\bar{\rho}_{\rm dcdm}\,,\end{aligned} \tag{2.7}$$

where the average over the momentum distribution is denoted by $\langle X\rangle = 1/\Gamma\cdot\int X\,{\rm d}\Gamma$. Here $\bar{\rho}_{\rm dr}$ is the sum of the energy densities of the two DR contributions, which evolve in the same way.

In [40] it was argued that in the limit $\epsilon \ll 1$ primarily interesting to us, the impact of the three-body decay on cosmological observables can be effectively mapped on an equivalent two-body decay model. We review the reasoning in the following. The impact of dark matter decay on the background evolution becomes negligible for $\epsilon \to 0$ since then $\langle 2E_{\rm dr}\rangle/M = \mathcal{O}(\epsilon)$ and $\langle E_{\rm wdm}\rangle/M = 1+\mathcal{O}(\epsilon)$. This implies that $\bar{\rho}_{\rm dr}$ becomes negligibly small and the total dark matter density $\bar{\rho}_{\rm dcdm}+\bar{\rho}_{\rm wdm}$ evolves approximately as if there was no decay. The same argument applies to the two-body decay, such that for both cases the background evolution is unaltered compared to ΛCDM for $\epsilon \ll 1$. Instead, the perturbations are responsible for the dominant effect on cosmological observables, capturing the heating of the WDM component produced in the decay. A fluid approximation for the WDM component that keeps track of the first two moments of the distribution function was introduced and validated against the full Boltzmann hierarchy for $\epsilon \ll 1$ in [36]. The impact of the decay is in this framework dominantly captured by an effective sound velocity, related to the adiabatic value $c_g^2 \equiv \dot{\bar{P}}_{\rm wdm}/\dot{\bar{\rho}}_{\rm wdm}$. For the three-body decay, it can be expressed as [40]

$$\begin{aligned}c_g^2 = &\left(\omega\left(5-\frac{\mathfrak{p}}{\bar{P}_{\rm wdm}}\right) - a\Gamma\frac{\bar{\rho}_{\rm dcdm}}{\bar{\rho}_{\rm wdm}}\frac{1}{\mathcal{H}M}\left\langle\frac{p_{\rm wdm}^2}{3E_{\rm wdm}}\right\rangle\right)\\ &\cdot\left(3(1+\omega) - a\Gamma\frac{\bar{\rho}_{\rm dcdm}}{\bar{\rho}_{\rm wdm}}\frac{1}{\mathcal{H}M}\langle E_{\rm wdm}\rangle\right)^{-1}\,,\end{aligned} \tag{2.8}$$

where $\mathfrak{p}$ is the pseudo-pressure [54]. The main difference to two-body decays is the appearance of averages involving the energy $E_{\rm wdm}$ and momentum $p_{\rm wdm}$ of the massive decay product over the decay spectrum, capturing the model-dependence. The two-body case is recovered by replacing $\langle E_{\rm wdm}\rangle \to E_{\text{2-body}} = (1-\epsilon)M$ and $\langle p_{\rm wdm}^2/(3E_{\rm wdm})\rangle \to p_{\text{2-body}}^2/(3E_{\text{2-body}}) = \epsilon^2 M/(3-3\epsilon)$.

The main idea of the mapping of cosmological constraints from two- to three-body decays is that models with a given value of c_g^2 will lead to (approximately) identical predictions of

JCAP01(2025)055

observables such as the matter power spectrum, since their impact is mostly captured by the sound velocity for small ϵ [36]. We thus consider a fictitious two-body decay model (with fictitious mass splitting ϵ') that leads to the same sound velocity as the three-body decay model (with actual mass splitting ϵ) of interest. To obtain this mapping, we note that both $\mathfrak{p}$ and ω are suppressed with $\mathcal{O}(\epsilon^2)$ so the numerator in eq. (2.8) is dominated by the second term. Additionally, the denominator is the same for the two- and three-body case at leading order in ϵ and thus the ratio of the sound velocities for each case can be written as

$$\frac{c_g^2|_{\text{3-body}}}{c_g^2|_{\text{2-body}}} = \frac{\langle p_{\text{wdm}}^2/3E_{\text{wdm}}\rangle}{p_{\text{2-body}}^2/3E_{\text{2-body}}}\,. \tag{2.9}$$

For the two-body decay, $p_{\text{2-body}}^2/3E_{\text{2-body}} = \epsilon'^2 M/(3-3\epsilon') \simeq \epsilon'^2 M/3$, while a more complicated dependence on ϵ occurs for the three-body decay, depending on the momentum distribution. Mapping cosmological constraints from two- to three-body decays corresponds to finding the value of ϵ' such that

$$c_g^2|_{\text{3-body}}(\epsilon) \stackrel{!}{=} c_g^2|_{\text{2-body}}(\epsilon')\,. \tag{2.10}$$

Inserting the explicit expressions for the sound velocities yields the desired mapping $\epsilon'(\epsilon)$. For example, when assuming a constant (momentum-independent) matrix element for the three-body decay, one obtains [40]

$$\epsilon'(\epsilon) = \sqrt{\frac{3}{5}}\epsilon + \mathcal{O}(\epsilon^2)\,. \tag{2.11}$$

We will apply in the next section this mapping procedure to a concrete particle physics model.

3 A minimal model of decaying cold dark matter

The SM does not contain candidates for CDM nor for WDM. Therefore, the model requires at least two new particle species, that have to be pseudo-degenerate in mass. It is plausible to consider that two particles with a small mass difference carry the same spin, therefore we will consider these two new particles to be Dirac fermions, denoted by N_1 and N_2, with masses of $m_{N_2} = M$ and $m_{N_1} = m \approx M(1-\epsilon)$. On the other hand, as discussed in section 2, the "dark radiation" consists of relativistic particles that have negligible interactions with visible matter after the onset of the recombination epoch. Notably, the SM contains particles fulfilling these properties: the active neutrinos. Therefore, in a minimal setup, one can identify the DR particles with the neutrinos.

To describe the interaction, we will use an effective field theory approach. The lowest dimensional operators involving N_1, N_2 and SM neutrinos are of the form

$$\mathcal{L} \sim (\bar{L}N_1)(\bar{N}_2 L) + \text{h.c.} \quad \text{or} \quad \mathcal{L} \sim (\bar{L}N_1)(\bar{N}_2^c L) + \text{h.c.}\,, \tag{3.1}$$

where $L = (\nu_L, e_L)$ is the SM lepton doublet, which includes the left-handed neutrino and electron fields. These six-dimensional operators lead to the decays $N_2 \to N_1\nu\bar{\nu}$ and $N_2 \to \bar{N}_1\nu\bar{\nu}$, and as discussed in section 2 can potentially solve the S_8 tension if $\Gamma \simeq 10^{-18} - 10^{-19}\,\text{s}^{-1}$ and $\epsilon \simeq 10^{-2} - 10^{-3}$. However, the same operators also generate decays into

JCAP01(2025)055

charged leptons, $N_2 \to N_1 e^- e^+$ or $N_2 \to \bar{N}_1 e^- e^+$, with comparable rate if kinematically accessible, and also the decay $N_2 \to N_1 \gamma$ at the one-loop level, with a rate suppressed by a factor $\mathcal{O}(10^{-3})$ [55]. Gamma-ray observations restrict the dark matter decay width to be $\Gamma_\gamma \lesssim 10^{-30}\,\mathrm{s}^{-1}$ [56–58] and positron flux measurements to be $\Gamma_{e^+} \lesssim 10^{-28}\,\mathrm{s}^{-1}$ [59–61]. Therefore, solving the S_8 tension with these two operators seems at odds with the gamma-ray and the positron observations.

In order to forbid these operators, we assign lepton number to $N_{1,2}$, corresponding to a global U(1) transformation for which $N_1 \to e^{i\alpha} N_1$ and $N_2 \to e^{i\alpha} N_2$. In addition, we need to introduce a second global U(1) symmetry, that transforms $N_1 \to e^{i\alpha} N_1$ and $N_2 \to e^{-i\alpha} N_2$, while all SM particles transform trivially under this symmetry. We will refer to the charge under this symmetry as "N-number". Note that the conservation of lepton number and the conservation of "N-number", ensure that not only both of the four-fermion interactions from eq. (3.1) are absent, but also similar four-fermion interactions where the lepton doublets are replaced by any other SM fermion fields. These symmetries are also compatible with Dirac mass terms $\mathcal{L}_{\rm mass} = -m_{N_1} \bar{N}_1 N_1 - m_{N_2} \bar{N}_2 N_2$ while forbidding any mass mixing terms (e.g. $\bar{N}_1 N_2$) or Majorana mass terms (i.e. $\bar{N}_i^c N_j$), such that N_1 and N_2 indeed correspond to Dirac fermion mass eigenstates. Finally, the symmetry $N_1 \to e^{i\alpha} N_1$ ensures the stability of N_1, since it is the lightest particle carrying "N-number".

The conservation of "N-number" and lepton number forbids the dimension-six operators in eq. (3.1). However, there exist higher dimensional operators allowed by the symmetries. The simplest one is the dimension-eight operator[1]

$$\mathcal{L}_{\rm int} = \frac{1}{\Lambda^4} \left(\bar{L} \tilde{H} P_R N_2\right) \left(\bar{L} \tilde{H} P_R N_1\right) + \text{h.c.}\,, \tag{3.2}$$

which leads after the electroweak symmetry breaking to the four-fermion interaction of $N_{1,2}$ and a neutrino pair, described by the effective Lagrangian

$$\mathcal{L}_{\rm eff} = \frac{v_{\rm EW}^2}{2\Lambda^4}\, \bar{\nu} P_R N_2\, \bar{\nu} P_R N_1 + \text{h.c.}\,. \tag{3.3}$$

This operator induces the decay

$$N_2 \to \bar{N}_1 \nu\nu\,, \tag{3.4}$$

involving two neutrinos in the final state, instead of a neutrino-antineutrino pair. We note that the hypothetical decay $N_2 \to \bar{N}_1 e^- e^-$ is allowed by the conservation of the "N-number" and the lepton number, but not by the conservation of the local U(1) electromagnetic symmetry. Further, the decay $N_2 \to \bar{N}_1 \gamma$ is not allowed by the conservation of the lepton number. Therefore, this scenario is a potentially viable DCDM scenario, since the rate for $N_2 \to N_1 \nu\nu$ could be in the ballpark of the values required to address the S_8 tension, while avoiding the constraints from gamma-ray and positron observations. Other, more suppressed, decay channels producing gamma-rays and positrons will be discussed in section 6.

[1] An analogous operator is given by $\bar{N}_1 N_2^c \bar{L}^c \tilde{H}^* \tilde{H}^\dagger L$. We focus on eq. (3.2) for definiteness here. There exist other lower-dimensional operators, e.g. $\bar{N}_i N_i H^\dagger H$, that however are irrelevant for DM decay.

JCAP01(2025)055

In order to determine the regions of the parameter space that is relevant for the S_8 tension, we first calculate the squared matrix element for $N_2 \to \bar{N}_1 \nu\nu$. We find

$$\overline{|\mathcal{M}|^2} = \frac{v_{\rm EW}^4}{2\Lambda^8} \left(2(k_1 \cdot p_1)(k_2 \cdot p_2) + 2(k_2 \cdot p_1)(k_1 \cdot p_2) - (k_1 \cdot k_2)(p_1 \cdot p_2) \right) , \tag{3.5}$$

where $k_{1,2}$ are the momenta of the neutrinos, $p_{1,2}$ the momenta of $N_{2,1}$, and we summed over the final state spins and averaged over the initial state spins. The differential decay rate reads, keeping the leading order in an expansion in small ϵ,

$$\frac{{\rm d}\Gamma_{N_2 \to N_1 \nu\nu}}{{\rm d}p_{\rm wdm}} = \frac{v_{\rm EW}^4}{1536\pi^3 \Lambda^8} p_{\rm wdm}^2 \left(p_{\rm wdm}^2 + 3M^2\epsilon^2 \right) , \tag{3.6}$$

and the total decay rate,

$$\Gamma_{N_2 \to N_1 \nu\nu} = \frac{v_{\rm EW}^4}{1280\pi^3 \Lambda^8} (\epsilon M)^5 . \tag{3.7}$$

Note the suppression by ϵ^5, arising partially from the marix element (ϵ^2) and the phase-space (ϵ^3). Thus, the suppression scale Λ of the effective interaction to produce a given lifetime τ is

$$\Lambda = \left(\frac{v_{\rm EW}^4}{1280\pi^3} \tau \, (\epsilon M)^5 \right)^{1/8} \approx 12\,{\rm TeV} \left(\frac{\tau}{100{\rm Gyrs}} \right)^{1/8} \left(\frac{\epsilon M}{\rm MeV} \right)^{5/8} . \tag{3.8}$$

We can finally translate cosmological constraints obtained for a two-body decay using the mapping derived in [40] and reviewed in section 2. For this purpose, we have to calculate

$$\langle p_{\rm wdm}^2 / 3E_{\rm wdm} \rangle = \frac{1}{\Gamma_{N_2 \to N_1 \nu\nu}} \int \frac{p_{\rm wdm}^2}{2E_{\rm wdm}} \frac{{\rm d}\Gamma_{N_2 \to N_1 \nu\nu}}{{\rm d}p_{\rm wdm}} {\rm d}p_{\rm wdm} , \tag{3.9}$$

where $E_{\rm wdm} = \sqrt{M^2(1-2\epsilon) + p_{\rm wdm}^2} \simeq M$. Using eq. (2.10), one can derive cosmological constraints on the three-body decay $N_2 \to \bar{N}_1 \nu\nu$ from a hypothetical two-body decay characterized by a fictitious mass splitting ϵ' given by

$$\epsilon'(\epsilon) \simeq \sqrt{\frac{13}{21}} \epsilon . \tag{3.10}$$

In figure 2 we show the cosmological constraints adapted to three-body decay and regions of the parameter space spanned by ϵ and τ that address the S_8 tension. For illustration, we also show contour lines in figure 2 of the suppression scale of the effective interaction operator eq. (3.2), at $\Lambda = 10\,{\rm TeV}$ and $50\,{\rm TeV}$, respectively. It would be interesting to investigate possible probes of the new particle species mediating the interaction of DM with neutrinos that are expected to exist at these scales. However, in this work we focus on the signatures of the decay itself while remaining agnostic about the origin of the effective interaction.

4 Constraints from the diffuse neutrino flux

The model discussed in section 3 produces a diffuse neutrino flux through the decays $N_2 \to \bar{N}_1 \nu\nu$ as well as $\bar{N}_2 \to N_1 \bar{\nu}\bar{\nu}$, thus providing a possible test of this solution of the S_8 tension.

JCAP01(2025)055

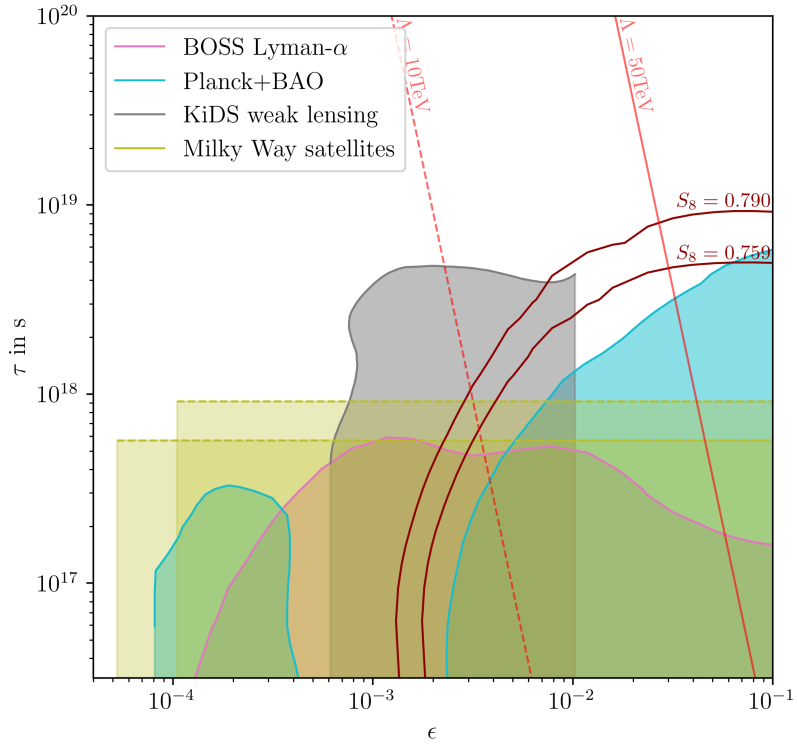

Figure 2. Same as figure 1, but for the minimal decaying cold dark matter scenario DCDM $\rightarrow$ WDM + DR_a + DR_b described in section 3. The plot also shows contours of the suppression scale $\Lambda = 10\,\mathrm{TeV}$ and $50\,\mathrm{TeV}$ of the dimension-eight operator eq. (3.2) inducing the decay, assuming $M = 0.3\,\mathrm{GeV}$.

Assuming that the bulk of the DM today is still in the form of cold dark matter (which is justified for the relevant lifetimes), the neutrino flux approximately reads

$$\frac{\mathrm{d}\Phi_\nu}{\mathrm{d}E_\nu} \simeq \frac{1}{4\pi}\frac{1}{\tau M}\frac{1}{3}\frac{\mathrm{d}N}{\mathrm{d}E_\nu} D(\Omega)\,, \tag{4.1}$$

where dN/dE_ν is the neutrino spectrum produced per DCDM decay normalized to one, and which is given in our model by

$$\frac{\mathrm{d}N}{\mathrm{d}E_\nu} = \frac{1}{\Gamma}\frac{\mathrm{d}\Gamma}{\mathrm{d}E_\nu} = \frac{30E_\nu^2(M\epsilon - E_\nu)^2}{M^5\epsilon^5}\,. \tag{4.2}$$

The energy spectrum of the neutrinos is shown for illustration in figure 3 for $\epsilon \ll 1$. Further, the factor 1/3 accounts for the three neutrino flavors, assuming that DM either decays into each flavor with equal rate, or that neutrino oscillations eventually cause all flavours to appear equally. Finally, the so-called D factor is defined as an integral of the DM density over the line of sight l in a given angular region in the sky

$$D(\Omega) = \int \mathrm{d}\Omega \int \rho(l)\,\mathrm{d}l\,, \tag{4.3}$$

and thus depends on the DM distribution. For concreteness, we adopt the value quoted in [62], $D(\Omega) = 2.65\cdot 10^{23}\mathrm{GeV/cm}^2$, which corresponds to a Navarro-Frenk-White (NFW) profile with

JCAP01(2025)055

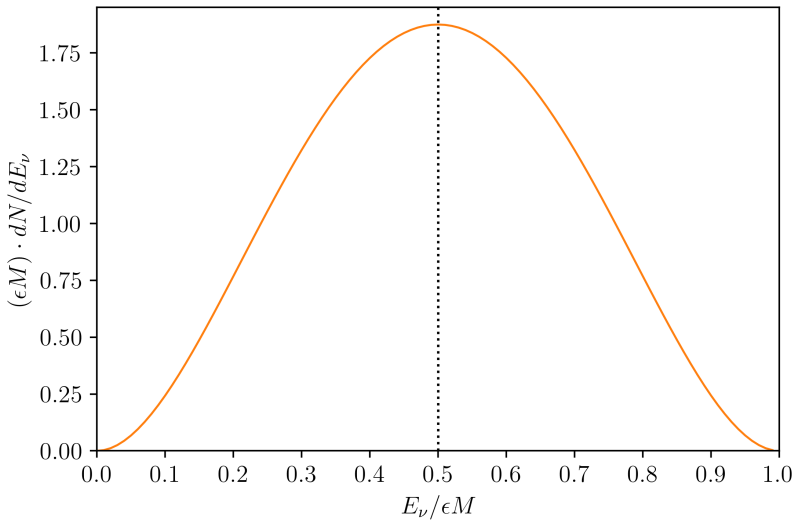

Figure 3. Neutrino spectrum $\mathrm{d}N/\mathrm{d}E_\nu$ produced by three-body decays $N_2 \to \bar{N}_1 \nu\nu$ for $\epsilon \ll 1$, as a function of the neutrino energy normalized to its maximum value ϵM.

slope parameter $\gamma = 1.2$ and scale radius $r_s = 20\,\mathrm{kpc}$, and a DM density $\rho = 0.4\mathrm{GeV/cm}^3$ at a distance $R_0 = 8.1\,\mathrm{kpc}$ from the Galactic center.

To the best of our knowledge, there are no published limits on the dark matter lifetime for this three-body decay spectrum (for other decay channels, see *e.g* [62]). We conservatively derive upper limits on the lifetime requiring that the flux generated in the decay does not exceed the measured flux. Concretely, we use the electron anti-neutrino flux measurements between 1.8 and 16.8 MeV from Borexino [63], between 8.3 and 30.8 MeV from KamLAND [64], as well as between 9.3 and 34.3 MeV from Super-Kamiokande (SK) [65]. Additionally, we recast SK limits for annihilating dark matter [66] for $10 - 200\,\mathrm{MeV}$, and translate them into decay limits (indicated by SK Ol. et al. in figure 4).

We show in figure 4 as shaded colored regions the constraints from neutrino flux measurements on DCDM within the parameter space spanned by (ϵ, τ), for two values of the DM mass: $M = 1\,\mathrm{GeV}$ (top) and $M = 0.3\,\mathrm{GeV}$ (bottom). We also show as thick red lines the values of parameters that could solve the S_8 tension. We find that neutrino experiments for these mass scales constrain values $\epsilon \gtrsim \mathcal{O}(10^{-2})$, corresponding to neutrino energies above $\simeq 10\,\mathrm{MeV}$, where neutrino detectors are most sensitive. The constraints from neutrino experiments are nicely complementary to the constraints from cosmology. Interestingly, we find an allowed window in parameter space for low masses $M \lesssim \mathrm{GeV}$, where low values of $S_8 \lesssim 0.8$, as preferred by various cosmological data sets, are allowed both by neutrino and cosmological constraints (see highlighted box in the lower panel of figure 4).

Future neutrino experiments like JUNO [67, 68], DUNE [69, 70] or Hyper-Kamiokande [71, 72] will close in on the parameter space of the model. Specifically, we show in figure 4 the projected sensitivity of JUNO to the model, recasting the sensitivity of JUNO to the decay $\chi \to \nu\bar{\nu}$ given in [67], and will explore regions of the parameter space that address the S_8 tension and which are allowed by current experiments.

JCAP01(2025)055

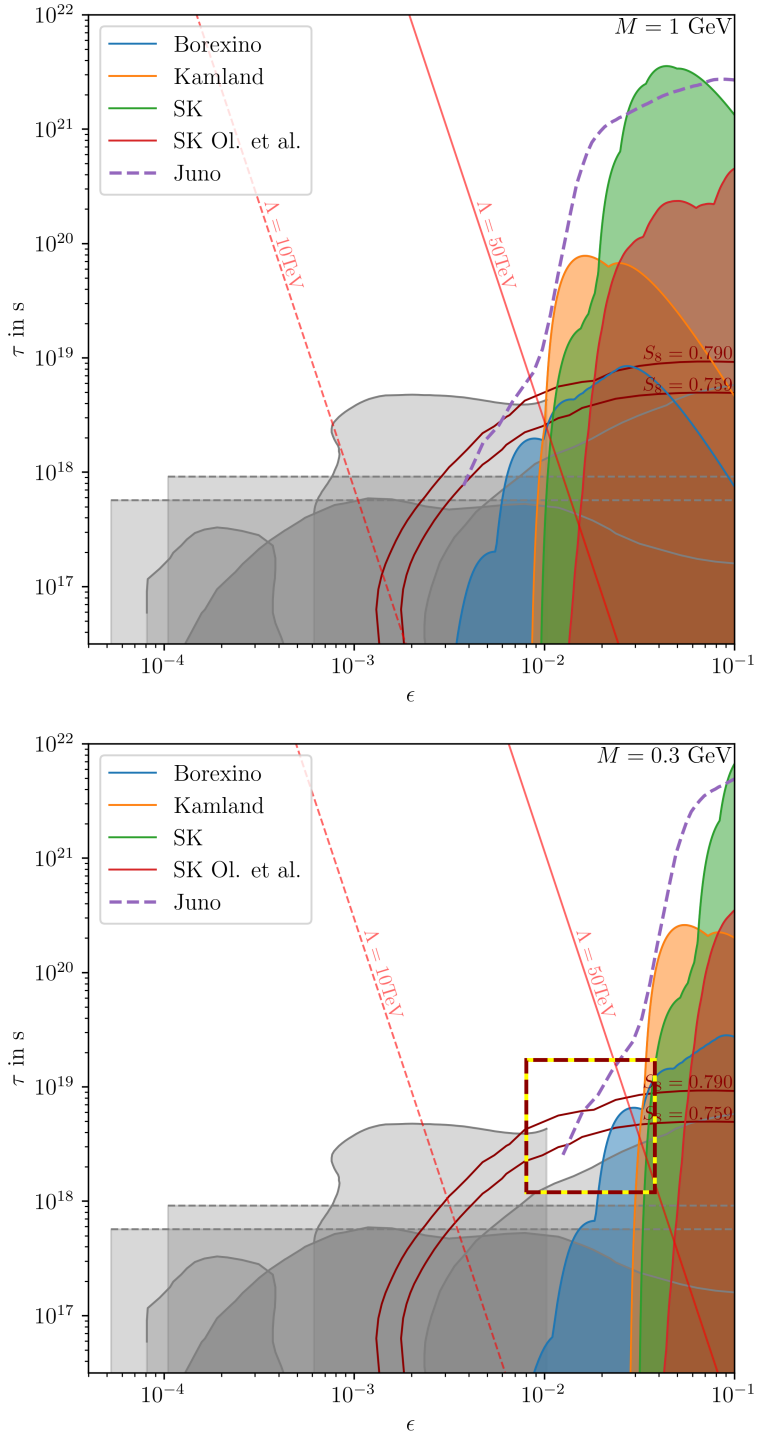

Figure 4. Allowed regions of the minimal decaying cold dark matter scenario DCDM $\rightarrow$ WDM + DR_a + DR_b described in section 3, for $M = 1\,\mathrm{GeV}$ (upper panel) and $M = 0.3\,\mathrm{GeV}$ (lower panel). The gray regions are excluded by cosmological observations (see section 3), and the colored regions are excluded by neutrino experiments (see section 4). The red thick lines indicate the region of parameter space that can address the S_8 tension, while thin lines show contours of the suppression scale $\Lambda = 10\,\mathrm{TeV}$ and $50\,\mathrm{TeV}$ of the dimension-eight operator eq. (3.2) inducing the decay.

JCAP01(2025)055

5 Dark matter production via freeze-in

The effective operator eq. (3.2) leading to the dark matter decay also leads to the production of dark matter particles via the processes $\nu\nu \to N_1 N_2$ and $\bar{\nu}\bar{\nu} \to \bar{N}_1 \bar{N}_2$ when the temperature of the Universe is $T_{\rm EW} \gtrsim T \gtrsim M$ (here, $T_{\rm EW} \simeq 160\,\text{GeV}$ is the temperature scale of electroweak symmetry breaking [73]). The values of the suppression scale favored by the DCDM solution to the S_8 tension are $\Lambda = \mathcal{O}(\text{TeV})$, which implies that the production process is very slow, and that the inverse annihilation processes have a negligible rate in the Universe (for details, see appendix D). Therefore, within the DCDM scenario considered here, dark matter could be produced via the freeze-in mechanism.

The evolution of the total dark matter yield Y, defined as $Y = n/s$, with n being the sum of the number densities N_1 and N_2 and s the entropy density, is given by [74, 75]

$$\frac{\mathrm{d}Y}{\mathrm{d}x} = \frac{1}{\sqrt{g_{\rm eff}} h_{\rm eff}} \sqrt{\frac{5}{\pi}} \frac{135 M_{\rm pl}}{4\pi^3 M} x^4 \frac{\gamma_{N_1 N_2}}{M^4}\,, \tag{5.1}$$

where $x = M/T$ and $\gamma_{N_1 N_2}$ is the DM production rate. The abundance of $\bar{N}_1$ and $\bar{N}_2$ produced via the corresponding charge-conjugated process is equal, such that the total DM yield is given by $2Y$. Furthermore, we checked that conversion processes among the two species can be neglected for freeze-in (see appendix B). We calculate $\gamma_{N_1 N_2}$ by performing the phase-space integration over the squared matrix element and over the neutrino distribution (see appendix B for details). Explicitly, it reads

$$\gamma_{N_1 N_2} = \frac{v_{\rm EW}^4 M^8}{256\pi^5 \Lambda^8} \frac{1}{x^8} \left(x^6 K_1(x)^2 + 2x^5 K_1(x) K_2(x) + (4 + x^2) x^4 K_2(x)^2 \right)\,, \tag{5.2}$$

with K_1 and K_2 modified Bessel functions of the second kind of order one and two, respectively. Notice the strong increase with temperature with $\gamma_{N_1 N_2} \propto T^8$ in the limit of $T \gg M$. This can be related to the increase of the cross section with center-of-mass energy, which is in turn related to the fact that the interaction is described by an effective four-fermion vertex. We have solved the Boltzmann equation, and we have determined the yield at $x \to \infty$, Y_∞. As initial condition, we assume an instant reheating of the universe at a temperature $T_{\rm rh} \leq T_{\rm EW}$, at which the dark matter yield is equal to zero. Relaxing the assumption of instant reheating could lead to additional contributions to the DM abundance, depending on the specific reheating model [76].

Finally, we calculate the total DM abundance today accounting for the equal yields of N_1, $\bar{N}_1$, N_2 and $\bar{N}_2$ from

$$\Omega_{\rm dm} h^2 \simeq \frac{2 M Y_\infty s_0}{\rho_{\rm crit,0}/h^2} \approx \frac{2.74 \cdot 10^8 \cdot Y_\infty \cdot 2M}{\text{GeV}}\,, \tag{5.3}$$

where $\rho_{\rm crit,0}$ and s_0 are the critical and entropy densities today, respectively.

In figure 5, we show the regions in parameter space (ϵ, τ) for which freeze-in production matches the value $\Omega h^2 = 0.12$ preferred by Planck [2], for $M = 1\,\text{GeV}$ and for various values of the reheating temperature $T_{\rm rh}$. As discussed above we limit ourselves to the regime $T_{\rm rh} < T_{\rm EW}$, which is realized below the hatched region. Efficient freeze-in production is possible only for $T_{\rm rh} \gtrsim M$, since otherwise the typical thermal energy of

JCAP01(2025)055

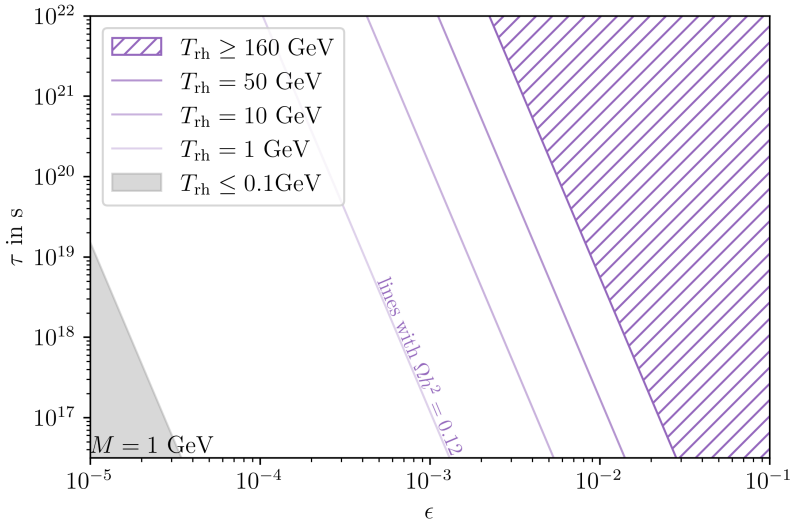

Figure 5. Values of lifetime and relative mass splitting for which the measured DM abundance $\Omega h^2 = 0.12$ can be reproduced via freeze-in, for $M = 1\,\text{GeV}$ and for different values of the reheating temperature below $T_{\rm EW} \simeq 160\,\text{GeV}$, due to the scatterings $\nu\nu \to N_1 N_2$ and $\bar{\nu}\bar{\nu} \to \bar{N}_1 \bar{N}_2$ induced by the operator eq. (3.2). In the hatched region the production is suppressed due to the large value of Λ, and in the grey region the production is suppressed due to the small phase space available.

neutrinos is not sufficient to produce DM particles. Specifically, for $T < M$ the Bessel functions entering the production rate eq. (5.2) feature an exponential Boltzmann suppression and thus we additionally exclude the region where $T_{\rm rh} < 0.1M$ is required to reach the relic abundance in gray. Notably, the values preferred by freeze-in production are in the ballpark of the values that address the S_8 tension, $\tau \simeq 10^2\,\text{Gyrs}$ and $\epsilon \simeq 10^{-2}$.

Production via freeze-in leads to an initial population of DM for which only 50% are in the form of the heavier state $N_2 + \bar{N}_2$ while 50% are already produced in the lighter state $N_1 + \bar{N}_1$. Thus, we have to generalize the results of our previous analyses with 100% DCDM. This can be easily done in the limit of $\tau \gg t_0$, which is always the case in the parameter space of interest, and we show in appendix B that the cosmological and astrophysical constraints derived previously can be mapped on the freeze-in scenario by simply re-scaling the lifetime by a factor of two.

Using this mapping, we overlay cosmological and astrophysical constraints with the requirement from producing the observed DM abundance via freeze-in for various viable reheating temperatures in figure 6. We note that for DM masses of order GeV, the region in parameter space relevant for the S_8 tension and compatible with constraints from neutrino flux measurements as well as CMB data is also compatible with freeze-in production. This is remarkable, since all interactions are generated by a single effective operator eq. (3.2) within the minimal model considered in this work. It is also interesting to note that this region of parameter space can be tested by upcoming neutrino experiments such as JUNO (dashed lines in figure 6) as well as future weak lensing surveys sensitive to S_8 [77].

JCAP01(2025)055

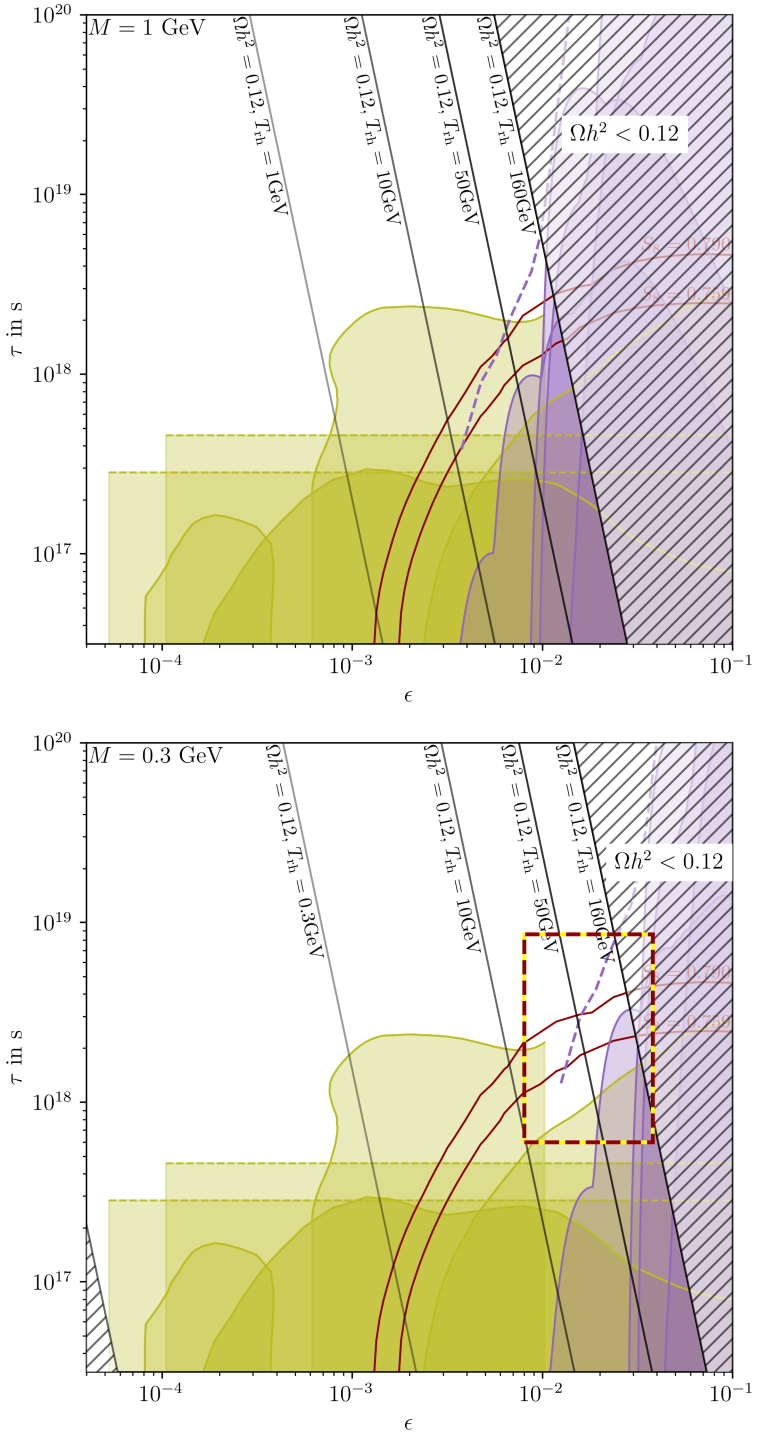

Figure 6. Recasting of figure 4, for the scenario where DM is produced via freeze-in. The black lines show contours for which $\Omega h^2 = 0.12$ for various reheating temperatures. In the hatched regions, the DM is underproduced (cf. figure 5). The box in the lower panel highlights the regions in parameter space where DCDM can address the S_8 tension and is compatible with all cosmological and experimental constraints, along with freeze-in production.

JCAP01(2025)055

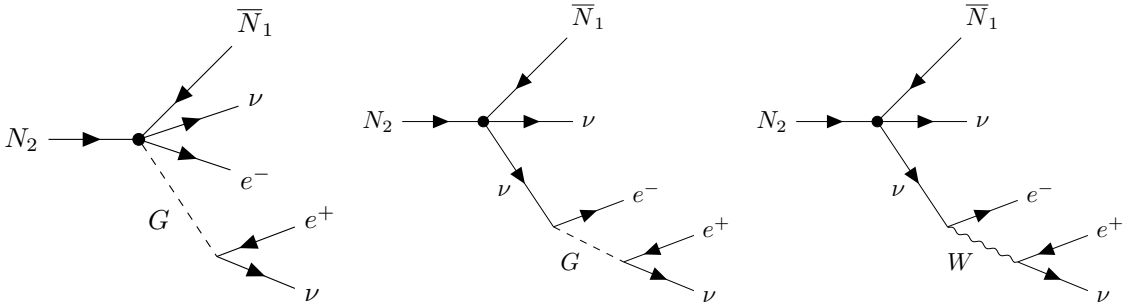

Figure 7. Decay producing an additional pair of charged particles via Goldstone and W boson processes. In unitary gauge, only the last diagram contributes, while in general only their sum is gauge independent.

6 Other possible signatures

In this section we discuss potential additional signatures that necessarily arise from the interaction described by the effective operator eq. (3.2).

6.1 Dark matter decay into charged particles

As discussed in section 3, DM decays into visible particles need to be strongly suppressed in order to satisfy positron and gamma-ray flux limits. Due to lepton number and charge conversation, the simplest form of such a decay is $N_2 \to \bar{N}_1 \nu e^- e^+ \nu$. This process can be mediated by either the Goldstone, arising from the Higgs-doublet, or the W boson and we show all contributing diagrams in figure 7. Note that in general only their sum is gauge independent (see appendix A).

Performing the five-body phase-space integration analytically in the limit $\epsilon \ll 1$, the resulting decay width reads

$$\Gamma_{N_2 \to \bar{N}_1 \nu\nu e^+ e^-} = \frac{v_{\rm EW}^4 g^4}{16 m_{\rm W}^4} \frac{(\epsilon M)^9}{7741440 \pi^7 \Lambda^8} \,. \tag{6.1}$$

The scaling with ϵ^9 results from the additional phase-space suppression which scales as ϵ^7 while the squared matrix element scales as ϵ^2 as for the three-body decay (see appendix A for details). Using eq. (3.7), we find that the branching fraction is

$$\frac{\Gamma_{N_2 \to \bar{N}_1 \nu\nu e^+ e^-}}{\Gamma_{N_2 \to \bar{N}_1 \nu\nu}} = \frac{(\epsilon M)^4}{6048 \pi^4 v_{\rm EW}^4} \approx 5 \cdot 10^{-28} \left(\frac{\epsilon M}{\rm MeV}\right)^4 . \tag{6.2}$$

We then find that the DCDM solution to the S_8 tension implies partial decay rates into electrons of order $\simeq 10^{-41}\,\mathrm{s}^{-1}$, which is far away from the sensitivity of current searches for cosmic electrons/positrons in the MeV range, $\Gamma_{e^+} \lesssim 10^{-27} - 10^{-29}\,\mathrm{s}^{-1}$ [59, 60].

6.2 Dark matter decay into photons

The interaction Lagrangian eq. (3.2) leads to an effective operator of the form

$$\mathcal{L}_{\rm eff} \supset \frac{v_{\rm EW}}{2\Lambda^4}\, h\, \bar{\nu} P_R N_2\, \bar{\nu} P_R N_1 + \text{h.c.}\,, \tag{6.3}$$

JCAP01(2025)055

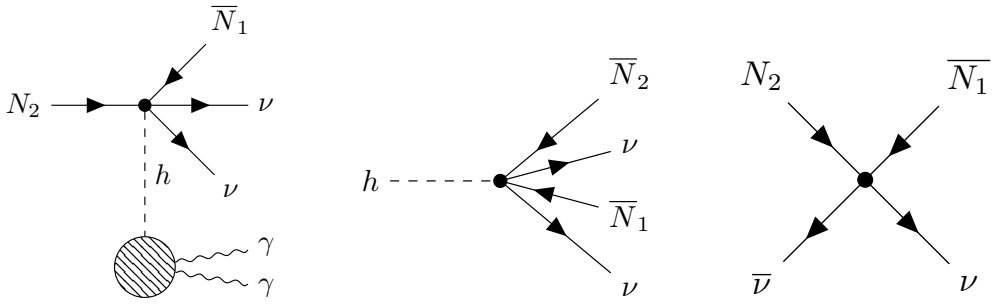

Figure 8. Diagrams leading to possible additional signatures of the DCDM model: dark matter decay with photons in the final state (left panel), Higgs invisible decay channel (middle panel), and neutrino-DM scattering (right panel).

which differs from eq. (3.3) in the substitution of the Higgs vacuum expectation value by a Higgs boson. The Higgs boson is too heavy to be produced on-shell, but it could decay off-shell into two photons as shown in figure 8 (left panel). The branching ratio reads

$$\frac{\Gamma_{N_2\to\bar{N}_1\nu\nu\gamma\gamma}}{\Gamma_{N_2\to\bar{N}_1\nu\nu}} \simeq \frac{\alpha_{\rm em}^2}{\pi^2}\frac{(\epsilon M)^8}{m_h^4 v_{\rm EW}^4}\,, \tag{6.4}$$

see appendix A for details. For the relevant parameter space with $\epsilon \simeq \mathcal{O}(10^{-2})$ and DCDM masses in the GeV range the branching ratio is thus very strongly suppressed, of the order of 10^{-39}. For the typical DCDM lifetimes required to address the S_8 tension, the expected width into photons is the order of $\Gamma_\gamma \simeq 10^{-39}\,{\rm s}^{-1}$, which is again far away from the sensitivity of current experiments, $\Gamma_\gamma \lesssim 10^{-23} - 10^{-30}\,{\rm s}^{-1}$ [56–58]. The four-body decay $N_2 \to \bar{N}_1\nu\nu\gamma$ associated to the five-body decay $N_2 \to \bar{N}_1\nu e^- e^+\nu$ upon closing the electron/positron lines in a loop is also expected to have a width well below the current sensitivity of experiments.

6.3 Invisible Higgs decay

The effective interaction eq. (6.3) derived from the interaction Lagrangian eq. (3.2) also implies a novel decay mode of the Higgs particle into DM particles and neutrinos, as shown in the middle of figure 8.

The decay width reads

$$\Gamma_{\rm h}^{\rm inv} = \frac{1}{4m_h}\frac{v_{\rm EW}^2}{30\pi^5\Lambda^8}\left(\frac{m_h}{4}\right)^8 \approx 1.37\cdot 10^{-20}{\rm MeV}\left(\frac{\rm MeV}{\epsilon M}\right)^5\left(\frac{100\,{\rm Gyrs}}{\tau}\right)\,, \tag{6.5}$$

which has been normalized to the typical values of ϵM and τ that address the S_8 tension. In view of the value of the Higgs decay width into SM final states, $\Gamma_{\rm h}^{\rm SM} \simeq 3.2\,{\rm MeV}$, and the current upper limit on the invisible decay width of the Higgs, ${\rm BR}_{h\to{\rm inv}} \lesssim 12\%$ [78], one concludes that this invisible decay is far below the current experimental sensitivity when $M \gtrsim 10\,{\rm MeV}$. For lower masses, we refer to a more detailed discussion in appendix D.

6.4 Neutrino-DM scattering

The effective interaction eq. (3.3) responsible for DCDM decay necessarily also gives rise to scattering between the DM particles and neutrinos, as shown in figure 8 on the right.

JCAP01(2025)055

More concretely, the neutrino can induce an exothermic or endothermic scattering with N_2 or N_1 respectively. These interactions can lead to a coupled neutrino-DM fluid exhibiting pressure such that DM fluctuations are damped on small scales, or even undergo dark acoustic oscillations. Thus, a neutrino-DM interaction can lead to observable deviations in the CMB, LSS, Lyman-α forest, and subhalo counts. In the literature, the case of an elastic neutrino-DM scattering has been extensively studied, leading to constraints on the cross section $\sigma_{\nu\mathrm{DM}}$, see e.g. [66, 79–89].

To estimate whether neutrino free-streaming is altered by our effective operator, we compare the scattering rate to the Hubble rate. As shown in appendix C the scattering rate in the thermal plasma around recombination scales as $\Gamma_\nu \propto T^4$, while the Hubble rate only scales as $H \propto T^2$. The strong temperature dependence implies that for temperatures relevant for cosmological limits, the scattering rate is severely suppressed, $\Gamma_\nu/H \ll 1$. Therefore, we do not expect any significant effect of the neutrino-DM scattering process in cosmology.

The neutrino-DM scattering cross section could also be constrained from the observation of high-energy neutrinos from astrophysical sources in neutrino telescopes, which imply that the neutrino fluxes have not been significantly attenuated by interactions with DM during their propagation from the production point to the Earth. The detection of high-energy neutrinos from the blazar TXS0506+056 by IceCube [90, 91] allows to set constraints on the neutrino-DM cross section at $E_\nu \simeq 290\,\mathrm{TeV}$. Conservative limits have been derived in [92], and have been improved including the effect of the dark matter spike around the central black hole of the blazar in [93, 94].

At very high neutrino energies, the cross section of the scattering process $N_2\bar{\nu} \to \bar{N}_1\nu$ reads

$$\sigma_{N_2\bar{\nu}\to\bar{N}_1\nu} \simeq \frac{v_{\mathrm{EW}}^4 M E_\nu}{128\pi\Lambda^8} \simeq 2\times10^{-49}\mathrm{cm}^2 \left(\frac{E_\nu}{290\mathrm{TeV}}\right)\left(\frac{\mathrm{MeV}}{\epsilon M}\right)^4\left(\frac{10^{-2}}{\epsilon}\right)\left(\frac{100\mathrm{Gyrs}}{\tau}\right), \quad (6.6)$$

and similarly for $N_1\bar{\nu} \to \bar{N}_2\nu$ (see appendix C for details). For typical parameters addressing the S_8 tension and DM masses above $\mathcal{O}(\mathrm{MeV})$ this is far below the upper limit derived from attenuation of high-energy neutrinos emitted from the blazar TXS0506+056 which are of order $10^{-29}\mathrm{cm}^2$ [93, 94]. Note that despite the large energy of the IceCube neutrinos, the validity condition $\sqrt{s} \ll \Lambda$ is satisfied for the relevant parameter values. The possibility of very low mass DM in the MeV range is discussed in appendix D.

Further constraints on the neutrino-DM scattering strength can be derived from the neutrinos detected from the supernova 1987A [95], that probe neutrino energies at the MeV scale, i.e. intermediate between CMB and IceCube energy scales. The upper limits of order $10^{-23}\mathrm{cm}^2$ as quoted in [93] are however somewhat weaker. Similarly, constraints can be derived in the same energy range from diffuse supernovae neutrinos affecting the DM density profile, as done recently in [96]. However, these also produce weaker limits for our model.

7 Conclusion and outlook

We have constructed and investigated a minimal model of decaying dark matter that can address the S_8 tension. The model consists of a cold dark matter particle that decays into a warm dark matter particle, quasi-degenerate in mass with the former, and two particles of "dark radiation", that we identify with the Standard Model neutrinos. This leads to a mild

JCAP01(2025)055

suppression of the matter power spectrum on small scales and at late times, in qualitative agreement with the S_8 measurements, if the cold dark matter lifetime is $\tau \simeq \mathcal{O}(10-100)$ Gyrs and the relative mass splitting between the cold and the warm dark matter particles is $\epsilon \simeq 10^{-2} - 10^{-3}$. In our model, both cold and warm dark matter candidates carry lepton number, and have opposite charges under a new global U(1) symmetry. This assignment allows the decay of the cold dark matter into warm dark matter and two neutrinos via a higher dimensional operator. On the other hand, the decays into charged leptons or into photons are very suppressed, thus evading the stringent limits on the lifetime of the decaying dark matter from cosmic electron/positron and gamma-ray experiments.

We have found that neutrino experiments like Borexino, KamLAND and Super-Kamiokande could detect signals of the diffuse neutrino flux generated in the decay, and that the upcoming JUNO neutrino observatory has the potential to probe the regions of parameter space addressing the S_8 tension if the DM mass is below $\simeq 1\,\text{GeV}$. Furthermore, the same interaction that mediates the three-body dark matter decay can also explain the abundance of dark matter by the freeze-in mechanism, via the process of conversion of two neutrinos into two dark matter particles in the Early Universe.

Finally, we have also investigated other possible signatures of the model, including the indirect detection of electron/positrons or gamma-rays from the decay, the invisible Higgs decay width, neutrino-dark matter scattering in the Early Universe, or the attenuation of the high-energy neutrino flux from blazars. For dark matter mass in the GeV mass range these signals are too faint to be detected, although they might be observed if the dark matter mass is in the MeV mass range. It would be interesting to explore possible UV completions of our decaying dark matter scenario including its impact on the DM production process, as well as whether any new particles could lead to additional signals in experiments. We leave this direction for future work.

Acknowledgments

We acknowledge support by the DFG Collaborative Research Institution Neutrinos and Dark Matter in Astro- and Particle Physics (SFB 1258) and the Excellence Cluster ORIGINS – EXC-2094 – 390783311.

A Five-body dark matter decays

A.1 Decay channel $N_2 \to \bar{N}_1 \nu e^- e^+ \nu$

In this section we provide some details for the $N_2 \to \bar{N}_1 \nu e^- e^+ \nu$ process discussed in section 6.1. Due to the Higgs-doublet $\tilde{H} = i\sigma_2 H^* = \left((v_{\text{EW}} + h - iG^0)/\sqrt{2}, -G^-\right)$, entering the effective interaction operator in eq. (3.2), DM can couple to an electron or positron via the longitudinal polarization of a W boson represented by the Goldstone boson G, e.g.

$$\mathcal{L}_{\text{eff}} \supset \frac{v_{\text{EW}}}{2\Lambda^4}\ \bar{\nu} P_R N_2\ e^+ P_R N_1 G^- + \text{h.c.}\,. \tag{A.1}$$

The Goldstone boson can then in turn decay into another charged lepton and neutrino pair, giving rise to a decay channel $N_2 \to \bar{N}_1 \nu e^- e^+ \nu$. The same decay can also be generated

JCAP01(2025)055

from $N_2 \to \bar{N}_1 \nu\nu$, where additionally one neutrino emits a Goldstone or W boson. All of these three contributions are shown in figure 7, where the individual diagrams depend on the choice of gauge fixing in general, while the complete matrix element should be gauge-fixing independent. To verify this, we can write down the matrix elements for each contribution in a general R_ξ gauge where the Goldstone propagator appearing in the first two diagrams takes the form $\frac{i}{\kappa_1^2 - \xi m_W^2}$. The W boson propagator needed for the last diagram is given by

$$\frac{-i}{\kappa_1^2 - m_W^2}\left[g_{\mu\nu} - (1-\xi)\frac{\kappa_{1\mu}\kappa_{1\nu}}{\kappa_1^2 - \xi m_W^2}\right] = \frac{-i g_{\mu\nu}}{\kappa_1^2 - m_W^2} + \frac{i\kappa_{1\mu}\kappa_{1\nu}}{\kappa_1^2 - m_W^2} - \frac{i\kappa_{1\mu}\kappa_{1\nu}}{\kappa_1^2 - \xi m_W^2}\,, \tag{A.2}$$

where we have rewritten it to recognise that only the last term depends on ξ and resembles a Goldstone propagator. In turn, we find that this term is responsible for cancelling both contributions from the first and second Goldstone process on the amplitude level, which is to be expected since the dependence on ξ needs to drop out to ensure gauge independence. Consequently, we can safely work in unitary gauge with $\xi \to \infty$ where the Goldstone contributions vanish naturally. Thus, the only left-over term now stems from the first two terms in eq. (A.2) from the W boson process and is given by

$$\begin{aligned} -i\mathcal{M} = \frac{1}{\Lambda^4}\frac{1}{\kappa_2^2}[\bar{u}(k_2)\gamma_\mu P_L v(l_2)]\left[\frac{m_W^2}{\kappa_1^2 - m_W^2} g^{\mu\nu} - \frac{\kappa_1^\mu \kappa_1^\nu}{\kappa_1^2 - m_W^2}\right] \\ \times \left([\bar{u}(l_1)\gamma_\nu P_L \cancel{\kappa_2} P_R u(p_1)][\bar{u}(k_1) P_R v(p_2)]\right. \\ \left. + [\bar{u}(k_1)\gamma_\nu P_L \cancel{\kappa_2} P_R u(p_1)][\bar{u}(l_1, t_1) P_R v(p_2)]\right)\,. \end{aligned} \tag{A.3}$$

Hereby, we chose $p_{1,2}$ for the momentum of the $N_{2,1}$ particles, $l_{1,2}$ for the e^- and e^+ and $k_{1,2}$ for the final state neutrinos. In the propagators, the W boson momentum is indicated by κ_1 and the neutrino momentum by $\kappa_2 = \kappa_1 + l_1$. Note that we do not include the exchange of both indistinguishable neutrinos ($k_1 \leftrightarrow k_2$) here which would cause an interference term to appear in the squared matrix element. Technically, this is justified if the leptons have different flavour, e.g. for $N_2 \to \bar{N}_1 \nu_\mu e^- e^+ \nu_e$, as generated from an effective interaction involving L_e and L_μ lepton doublets. Since the resulting decay width is many orders of magnitudes below the relevant limits, we expect that this is also the case for $N_2 \to \bar{N}_1 \nu_e e^- e^+ \nu_e$, provided the effective interaction strength is comparable for all flavour combinations. The squared matrix element with this simplification and the limit of $m_{\nu,e} \to 0$ and $m_W \to \infty$, then takes the form

$$\begin{aligned} \overline{|\mathcal{M}|^2} = \frac{v_{\mathrm{EW}}^4 g^4}{\Lambda^8 \kappa_2^4 m_{\mathrm{W}}^4} \left(4(k_2\cdot l_1)(k_1\cdot p_1)(\kappa_2\cdot l_2)(\kappa_2\cdot p_2) + 4(k_2\cdot l_1)(k_1\cdot p_2)(\kappa_2\cdot l_2)(\kappa_2\cdot p_1)\right. \\ - 2\kappa_2^2(k_2\cdot l_1)(k_1\cdot p_2)(l_2\cdot p_1) - 2\kappa_2^2(k_2\cdot l_1)(k_1\cdot p_1)(l_2\cdot p_2) \\ \left. - 2(p_1\cdot p_2)(\kappa_2\cdot k_1)(k_2\cdot l_1)(\kappa_2\cdot l_2) + \kappa_2^2(p_1\cdot p_2)(k_1\cdot l_2)(k_2\cdot l_1)\right)\,, \end{aligned} \tag{A.4}$$

where we made use of FeynCalc [97]. Note, that the W boson mass drops out because of $m_{\mathrm{W}} = v_{\mathrm{EW}} g/2$, where g is the $\mathrm{SU}(2)_L$ gauge coupling constant.

For the decay width, we have to compute the 5-body phase-space integral $\mathrm{d}\Phi_5$ over the matrix element

$$\Gamma_{N_2 \to \bar{N}_1 \nu\nu e^+ e^-} = \frac{1}{2M}\overline{|\mathcal{M}|^2} \int \mathrm{d}\Phi_5(p_1; p_2, k_1, k_2, l_1, l_2). \tag{A.5}$$

JCAP01(2025)055

Splitting the phase-space in two, we can instead calculate two subsequent three-body decays [78] $N_2 \to \bar{N}_1 \nu\nu$ and $\nu \to e^- e^+ \nu$ with

$$\overline{|\mathcal{M}|^2}\, \mathrm{d}\Phi_5 = \frac{1}{2\pi} \overline{|\mathcal{M}|^2}\, \mathrm{d}\Phi_3(q; l_1, l_2, k_2)\, \mathrm{d}\Phi_3(p_1; p_2, k_1, q)\, \mathrm{d}q^2\,, \tag{A.6}$$

where the virtual neutrino has a "mass" of q^2. First, we perform a tensor decomposition

$$l_1^\mu l_2^\nu k_2^\rho = q^\mu g^{\nu\rho} t_1(q, l_1, l_2, k_2) + q^\mu q^\nu q^\rho t_2(q, l_1, l_2, k_2) + (\mu \leftrightarrow \nu \leftrightarrow \rho)\,, \tag{A.7}$$

where $t_i(q, l_1, l_2, k_2)$ represent functions with all momenta contracted in scalar products. Thus, we can factorise the matrix element into one part depending on the first decay with momenta p_1, p_2, k_1 and one part depending on the second decay with l_1, l_2, k_2, where all momenta are contracted among themselves or with q. Eq. (A.6) can now be written as

$$\begin{aligned} &\frac{1}{(2\pi)\Lambda^8} \left(2(k_1 \cdot p_1)(q \cdot p_2) + 2(k_1 \cdot p_2)(q \cdot p_1) - (p_1 \cdot p_2)(q \cdot k_1)\right) \mathrm{d}\Phi_3(p_1; p_2, k_1, q) \\ &\qquad \times 2(k_2 \cdot l_1)(l_2 \cdot q)\, \mathrm{d}\Phi_3(q; l_1, l_2, k_2) \times \frac{\mathrm{d}q^2}{q^4}, \end{aligned} \tag{A.8}$$

and we can perform each three-body decay independently. For $\nu \to e^- e^+ \nu$, we can assume that the mass of the decay products are negligible and arrive at

$$\int 2(k_2 \cdot l_1)(l_2 \cdot q)\, \mathrm{d}\Phi_3(q; l_1, l_2, k_2) = \frac{q^6}{(2\pi)^3 \cdot 48}\,. \tag{A.9}$$

For $N_2 \to \bar{N}_1 \nu\nu$ we can expand in $\epsilon \ll 1$ and assume that $\bar{N}_1$ will be at rest at first order in ϵ, while the neutrinos have a momentum of the order ϵM. With this simplification, the integral takes the form

$$\begin{aligned} &\int \left(\, 2(k_1 \cdot p_1)(q \cdot p_2) + 2(k_1 \cdot p_2)(q \cdot p_1) - (p_1 \cdot p_2)(q \cdot k_1) \,\right) \mathrm{d}\Phi_3(p_1; p_2, k_1, q) \\ &\quad = \frac{M}{(2\pi)^3 \cdot 40} \cdot \Bigg[\sqrt{M^2\epsilon^2 - q^2}\left(-9M^2\epsilon^2 q^2 + 2M^4\epsilon^4 - 8q^4\right) \\ &\qquad\qquad + 15M\epsilon q^4 \ln \frac{\sqrt{M^2\epsilon^2 - q^2} + M\epsilon}{q}\Bigg] \Theta(q^2)\Theta\left(\sqrt{q^2} - \epsilon M\right)\,. \end{aligned} \tag{A.10}$$

Now, the q^2 integration can be done with $q^2_{\mathrm{min}} = 0$ and $q^2_{\mathrm{max}} = (\epsilon M)^2$ and we have

$$\int \mathrm{d}\Phi_5 \overline{|\mathcal{M}|^2} = \frac{M(\epsilon M)^9}{30240 \cdot (2\pi)^7 \Lambda^8}\,. \tag{A.11}$$

This result multiplied by $1/(2M)$ gives then the final decay width in eq. (6.1).

A.2 Decay channel into photons

In this section we give some details for the $N_2 \to \bar{N}_1 \nu\nu\gamma\gamma$ decay discussed in section 6.2. The decay involves a virtual Higgs boson decaying via $h^* \to \gamma\gamma$. This well-known process [98–102] can be characterized by a contribution to the matrix element from Higgs decay given by [101]

$$\mathcal{M}_{h^* \to \gamma\gamma} = \frac{2e^2}{(4\pi)^2 v_{\mathrm{EW}}} F(q^2)\left(q_1 \cdot q_2 g^{\mu\nu} - q_1^\nu q_2^\mu\right) \epsilon_\mu(q_1)\epsilon_\nu(q_2)\,, \tag{A.12}$$

JCAP01(2025)055

where e is the electromagnetic gauge coupling constant, q_i are the photon four-momenta, $q = q_1 + q_2$ that of the Higgs, and $F(q^2)$ is a loop factor. The virtuality q^2 takes the role of the Higgs "mass" for off-shell Higgs decay. Since the decay is dominated by W and top-quark contributions, and $q^2 = \mathcal{O}(\epsilon M)^2 \ll m_W^2, m_t^2$, the loop factor approaches a constant value corresponding to the heavy-top/W limit. With these simplifications, $|F|^2 \simeq 27.3$. The full squared matrix element for the process $N_2 \to \bar{N}_1 \nu\nu h^* \to \bar{N}_1 \nu\nu\gamma\gamma$ is in the limit $q^2 \ll m_h^2$ given by

$$\overline{|\mathcal{M}|^2}_{N_2 \to \bar{N}_1 \nu\nu\gamma\gamma} = \frac{\alpha_{\rm em}^2 |F|^2 \, (q_1 \cdot q_2)^2}{4\pi^2 m_h^4 v_{\rm EW}^4} \overline{|\mathcal{M}|^2}_{N_2 \to \bar{N}_1 \nu\nu} \,, \tag{A.13}$$

where $\alpha_{\rm em} = e^2/(4\pi)$ is the fine-structure constant, m_h the Higgs mass, and the last factor stands for eq. (3.5). Similarly to before, the photon momenta q_i can only be of the order $\mathcal{O}(\epsilon M)$ since most of the available energy in the N_2-decay is transferred to the rest mass of the daughter particle $\bar{N}_1$. For $\epsilon \ll 1$, the matrix element $\overline{|\mathcal{M}|^2}_{N_2 \to \bar{N}_1 \nu\nu\gamma\gamma}$ is suppressed by a factor ϵ^4 compared to $\overline{|\mathcal{M}|^2}_{N_2 \to \bar{N}_1 \nu\nu}$. Furthermore, the five-body phase-space leads to an additional suppression by a factor ϵ^4 as compared to the three-body decay, as well as an additional $1/\pi^2$ factor. Overall, this allows us to estimate the branching fraction as given in eq. (6.4), where we counted $|F|^2/\pi^2$ as order unity for simplicity.

B Dark matter production via freeze-in

For the DM production rate we have to solve

$$\gamma_{N_1 N_2} \equiv 2 \int \mathrm{d}\Pi_{k_1} \, \mathrm{d}\Pi_{k_2} \, \mathrm{d}\Pi_{p_1} \, \mathrm{d}\Pi_{p_2} (2\pi)^4 \delta^{(4)}(k_1 + k_2 - p_1 - p_2) \overline{|\mathcal{M}|^2}_{\nu\nu \to N_1 N_2} f_\nu(k_1) f_\nu(k_2) \,, \tag{B.1}$$

where $f_\nu(k) = 1/(e^{k/T} + 1)$ since neutrinos belong to the SM thermal bath at the relevant temperatures. Following [75] the integrals over $N_{1,2}$ momenta $p_{1,2}$ and neutrino momenta $k_{1,2}$ can be evaluated, leaving an integration over the squared center-of-mass energy $s = (k_1 + k_2)^2 = (p_1 + p_2)^2$ as well as the angle between e.g. the spatial momenta of k_1 and p_1,

$$\gamma_{N_1 N_2} = \frac{T}{8 \cdot 32\pi^6} \int \mathrm{d}s \, \frac{p_{\nu\nu} p_{N_1 N_2}}{\sqrt{s}} \, K_1\left(\frac{\sqrt{s}}{T}\right) \int \mathrm{d}\Omega \, \overline{|\mathcal{M}|^2}_{\nu\nu \to N_1 N_2} \,, \tag{B.2}$$

with K_1 being the modified Bessel function of the second kind of order one and

$$p_{ij} \equiv \frac{\sqrt{s - (m_i + m_j)^2}\sqrt{s - (m_i - m_j)^2}}{2\sqrt{s}} \,. \tag{B.3}$$

Using eq. (3.3) we obtain

$$\overline{|\mathcal{M}|^2}_{\nu\nu \to N_1 N_2} = \frac{v_{\rm EW}^4}{4\Lambda^8} \left(2(k_1 \cdot p_2)(k_2 \cdot p_1) + 2(k_1 \cdot p_1)(k_2 \cdot p_2) - (k_1 \cdot k_2)(p_1 \cdot p_2)\right) \,. \tag{B.4}$$

We assume $m \simeq M$, which is a valid approximation for small mass splitting $M - m \simeq \epsilon M \ll M$ since only temperatures $T \gtrsim M \gg \epsilon M$ are relevant for freeze-in. Then, we find

$$\int \mathrm{d}\Omega \, \overline{|\mathcal{M}|^2}_{\nu\nu \to N_1 N_2} = \frac{\pi}{12} \frac{v_{\rm EW}^4}{\Lambda^8} s(2M^2 + s) \,. \tag{B.5}$$

JCAP01(2025)055

Furthermore, $p_{\nu\nu} = \sqrt{s}/2$ and $p_{N_1N_2} = \sqrt{s-4M^2}/2$ as well as $s \geq 4M^2$ in the limit of small mass splitting $m \simeq M$. Performing the remaining integral over s from $4M^2$ to ∞ in eq. (B.2) then reproduces eq. (5.2).

Freeze-in via $\nu\nu \to N_1N_2$ leads to equal initial abundances of N_1 and N_2. One may wonder whether conversion processes may alter the relative abundances. Clearly, the decay process $N_2 \to \bar{N}_1\nu\nu$ itself is irrelevant in the Early Universe due to the cosmological DCDM lifetime we consider. However, conversions could also be mediated by scatterings of e.g. the form $N_2\bar{\nu} \to \bar{N}_1\nu$. Nevertheless, at temperatures $T \gg \epsilon M$, the rate of this and its inverse process is practically identical due to the mass splitting being negligible at these scales. Therefore, they would not change the relative abundance of $N_2 + \bar{N}_2$ versus $N_1 + \bar{N}_1$ particles even if they would occur at sizeable rates. For $T \ll \epsilon M$, the mass splitting becomes relevant, and would lead to a preference of the de-excitation process $N_2\bar{\nu} \to \bar{N}_1\nu$ over its inverse. However, we checked that its rate is strongly suppressed compared to the Hubble rate at these low temperatures. In conclusion, we can neglect conversion processes.

Lastly, the equal initial abundances of $N_1 + \bar{N}_1$ and $N_2 + \bar{N}_2$ also causes only 50% of DM to decay which we have to account for in our previous analyses. From the point of view of cosmological observations, the initial $N_1 + \bar{N}_1$ population acts as a component of stable cold dark matter (SCDM), since its velocity distribution inherited by the freeze-in process is negligibly small at around the recombination epoch. Therefore, we need to consider in general three distinct DM populations, being DCDM, WDM and SCDM, corresponding to $N_2 + \bar{N}_2$, $N_1 + \bar{N}_1$ produced via DCDM decay, and the initial $N_1 + \bar{N}_1$ population, respectively. At any given time the fraction of DM in the form of DCDM, WDM and SCDM is $0.5e^{-t/\tau}$, $0.5(1 - e^{-t/\tau})$ and 0.5, respectively (assuming $m \simeq M$,i.e. $\epsilon \ll 1$, as before). Since the DCDM lifetimes $\tau \simeq 10^2\,\mathrm{Gyrs}$ that we are interested in are somewhat above the age of the Universe t_0. It is not necessary to track the three components separately in this case, but it is sufficient to consider the total CDM density given by the sum of DCDM and SCDM populations. In particular,

$$\begin{aligned}
\rho_{\mathrm{cdm}} &= \rho_{N_1+\bar{N}_1,\mathrm{initial}} + \rho_{N_2+\bar{N}_2} = \frac{1}{2}\rho_0 a^{-3} + \frac{1}{2}\rho_0 a^{-3} e^{-t_0/\tau} \approx \rho_0 a^{-3}\left(1 - \frac{t_0}{2\tau}\right), \\
\rho_{\mathrm{wdm}} &= \rho_{N_1+\bar{N}_1,\mathrm{decay}} = \frac{1}{2}\rho_0 a^{-3}\left(1 - e^{-t_0/\tau}\right) \approx \rho_0 a^{-3}\frac{t_0}{2\tau},
\end{aligned} \tag{B.6}$$

where we expanded for $\tau \gg t_0$ in the last expressions in each line, and ρ_0 stands for the total DM density today. This can be compared to a corresponding model in which initially only the heavier state is present, and with lifetime denoted by τ'. The populations of cold and warm dark matter are then given by

$$\begin{aligned}
\rho_{\mathrm{cdm}} &= \rho_0 a^{-3} e^{-t_0/\tau'} \approx \rho_0 a^{-3}\left(1 - \frac{t_0}{\tau'}\right), \\
\rho_{\mathrm{wdm}} &= \rho_0 a^{-3}\left(1 - e^{-t_0/\tau'}\right) \approx \rho_0 a^{-3}\frac{t_0}{\tau'}.
\end{aligned} \tag{B.7}$$

Thus we see that for $\tau \gg t_0$ both setups can be mapped to each other when identifying $\tau' \equiv 2\tau$.

JCAP01(2025)055

C Dark matter-neutrino scatterings

Calculating the cross section for the $N_2\bar{\nu} \to N_1\nu$ and analogously for the inverse process yields

$$\sigma_{N_2\bar{\nu}\to\bar{N}_1\nu} = \frac{v_{\rm EW}^4}{256\pi\Lambda^8}\frac{(s-m^2)^2}{s} \quad \text{and} \tag{C.1}$$

$$\sigma_{N_1\bar{\nu}\to\bar{N}_2\nu} = \frac{v_{\rm EW}^4}{256\pi\Lambda^8}\frac{(s-M^2)^2}{s}\,, \tag{C.2}$$

where s is the square of the center-of-mass energy and we assumed massless neutrinos. As long as the effective four-fermion interaction is applicable (i.e. for $\sqrt{s} \ll \Lambda$), we thus find a scaling with s, as expected on dimensional grounds. For $N_2\bar{\nu} \to N_1\nu$ one has $s \simeq M^2 + 2ME_\nu$ when assuming the $\bar{N}_2$ to be non-relativistic. This can be assumed in the Early Universe for temperatures $T \ll M$. In this regime, the cross section depends on the masses and the neutrino energy, and thus temperature, with $E_\nu \sim T$. For $E_\nu \gg \epsilon M$, $\sigma_{N_2\bar{\nu}\leftrightarrow\bar{N}_1\nu} \propto s \propto E_\nu^1$, and the mass splitting between N_2 and N_1 can be neglected, such that the scattering can be considered effectively as elastic. For $E_\nu \ll \epsilon M$, we have $\sigma_{N_2\bar{\nu}\to\bar{N}_1\nu} \propto (\epsilon M)^2$ for the de-excitation, while the backward reaction is kinematically forbidden. In this regime, the scattering is strongly inelastic since the mass splitting of the DM particles dominates over the neutrino energy.

Assuming that DM is dominantly comprised of the heavier N_2 particles in the Early Universe, the neutrino scattering rate for $T \ll M$ can be estimated as

$$\Gamma_\nu = \sigma_{N_2\bar{\nu}\to\bar{N}_1\nu} \cdot v \cdot n_{N_2}\,, \tag{C.3}$$

where $n_{N_2} = \rho_{\rm DM}/M$ with $\rho_{\rm DM} \propto a^{-3} \propto T^3$ being the non-relativistic DM density and relative velocity $v \approx 1$. This can be compared to the usual Hubble rate $H \propto T^2$ to quantify whether the scattering may impact neutrino free-streaming. We show the ratio Γ_ν/H versus the neutrino energy $E_\nu \sim T$ in figure 9 for $M = 1\,\text{GeV}$, $\epsilon = 10^{-4}$ and $\tau = 100\,\text{Gyrs}$ (blue line). For $E_\nu \ll \epsilon M$ one has $\sigma_{N_2\bar{\nu}\to\bar{N}_1\nu} \propto E_\nu^0$ such that $\Gamma_\nu/H \propto T \sim E_\nu$ while for $E_\nu \gg \epsilon M$ the scaling $\sigma_{N_2\bar{\nu}\to\bar{N}_1\nu} \propto E_\nu^1$ implies $\Gamma_\nu/H \propto T^2 \sim E_\nu^2$. For illustration, we also show the scattering rate that would result from the inverse process $N_1\bar{\nu} \to \bar{N}_2\nu$ when assuming all of DM would be in the form of N_1 (faint orange line). While we do not consider this scenario further, we note that both rates become equal for $E_\nu \gg \epsilon M$, illustrating the effective elasticity in this limit. We also display constraints on neutrino-DM scattering from CMB and BAO observations [80] in figure 9. We stress that these constraints are obtained assuming purely *elastic* scattering, and are thus comparable to the model studied here only for $E_\nu \gg \epsilon M$. In this context, constraints are commonly expressed in terms of the dimensionless ratio

$$u_{\nu\rm DM} = \frac{\sigma_{\nu\rm DM}}{\sigma_T}\left(\frac{M}{100\text{GeV}}\right)^{-1}\,, \tag{C.4}$$

where σ_T is the Thompson cross section. In [80] a dependence $\sigma_{\nu\rm DM} \propto T^k$ was assumed, finding upper limits $\log_{10}(u_{\nu\rm DM}) \lesssim -5$ for $k = 0$ and $\log_{10}(u_{\nu\rm DM}) \lesssim -15$ for $k = 2$. We show these two upper limits in figure 9 in green solid and dashed lines, respectively. They both fall below $\Gamma_\nu/H \lesssim 1$ at energy scales $\mathcal{O}(0.1)\,\text{keV}$. This can be related to the fact that the small angular scales used in the CMB analysis of [80] enter the horizon when the temperature of the

JCAP01(2025)055

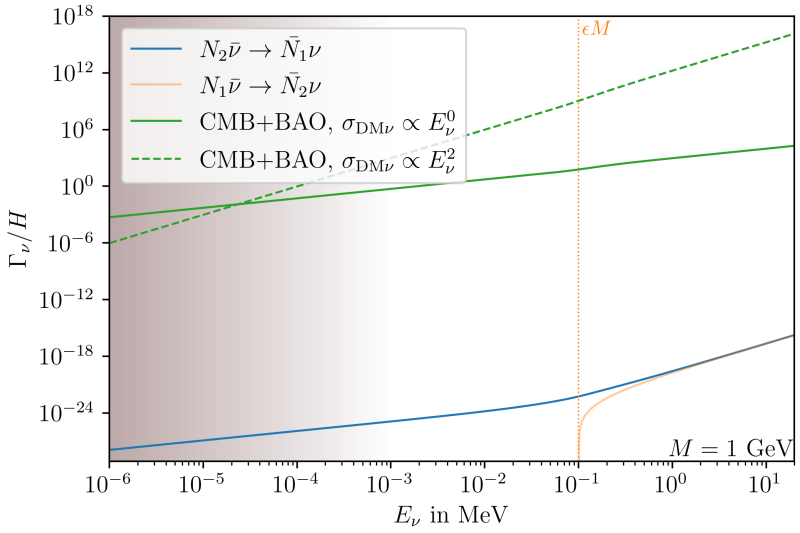

Figure 9. Ratio of the neutrino scattering rate and Hubble parameter versus the typical thermal neutrino energy $E_\nu \sim T$. In blue, the scattering rate for $N_2\bar{\nu} \to \bar{N}_1\nu$ is shown for typical parameter values $M = 1\,\mathrm{GeV}$, $\epsilon = 10^{-4}$ and $\tau = 100\,\mathrm{Gyrs}$. For comparison, we display limits on the elastic neutrino-DM cross section $\sigma_{\mathrm{DM}\nu}$ from [80] based on CMB and BAO data. The shaded region on the left indicates the energy regime that is relevant for CMB constraints.

thermal bath was around these energy scales. We observe that the neutrino-DM scattering rate predicted by the DCDM model under consideration is suppressed by many orders of magnitude in this temperature regime and consequently can be neglected.

D Decaying light dark matter

So far we focused on the DM mass range $M \simeq \mathcal{O}(\mathrm{GeV})$, for which the suppression scale Λ of the effective operator mediating DCDM decay lies in the multi-TeV range. Here, we discuss the low-mass regime with $M \simeq \mathcal{O}(\mathrm{MeV})$. Using eq. (3.8) to rewrite Λ as

$$\Lambda \simeq 160\mathrm{GeV} \left(\frac{\tau}{100\mathrm{Gyrs}} \left(\frac{\epsilon M}{10^{-3} \cdot 1\mathrm{MeV}} \right)^5 \right)^{1/8} , \tag{D.1}$$

implies that the typical interaction strength $\propto 1/\Lambda^8$ is enhanced. For even lower masses one would have $\Lambda \ll v_{\mathrm{EW}}$, which indicates that an EFT approach within the broken phase should be used. Thus, while the low-mass regime can boost some signatures, it is constrained by the validity of the EFT description.

In figure 10 we show the neutrino-DM scattering cross section for $M = 1\,\mathrm{MeV}$ and see that IceCube limits can put relevant constraints on DCDM in the low-mass regime. The cross section is shown only for $\sqrt{s} < \Lambda$ to ensure EFT validity and additionally, we checked that the cross section satisfies the unitarity bound. The resulting constraints can be seen in green in figure 11. Similarly, for invisible Higgs decay, we find non-trivial constraints when assuming that the EFT description remains valid for $\Lambda < v_{\mathrm{EW}}$, as illustrated in blue in figure 11. However, in red we also show the line where $\Lambda = v_{\mathrm{EW}}$. Since the momentum transfer for the

JCAP01(2025)055

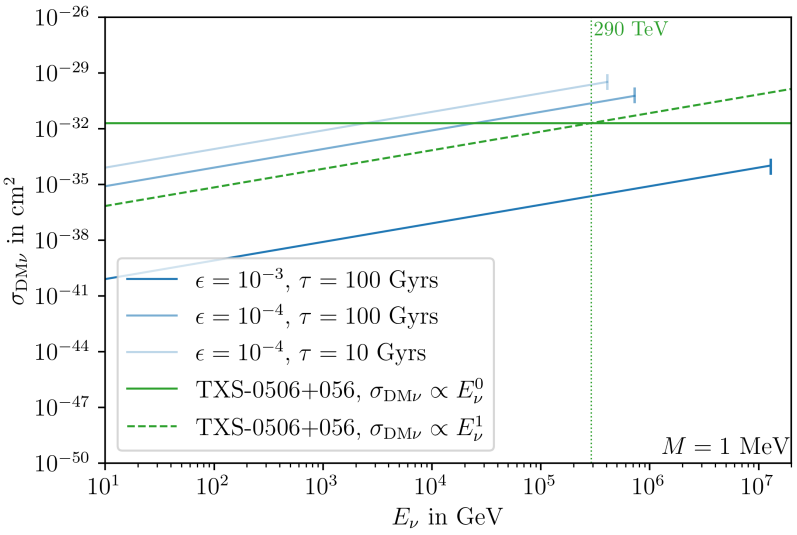

Figure 10. Cross section of neutrino-DM scattering for $M = 1\,\mathrm{MeV}$ and different ϵ and τ values in shades of blue. In green, constraints derived from IceCube observations of high-energy neutrinos observed from the direction of TXS-0506+056 are shown [93].

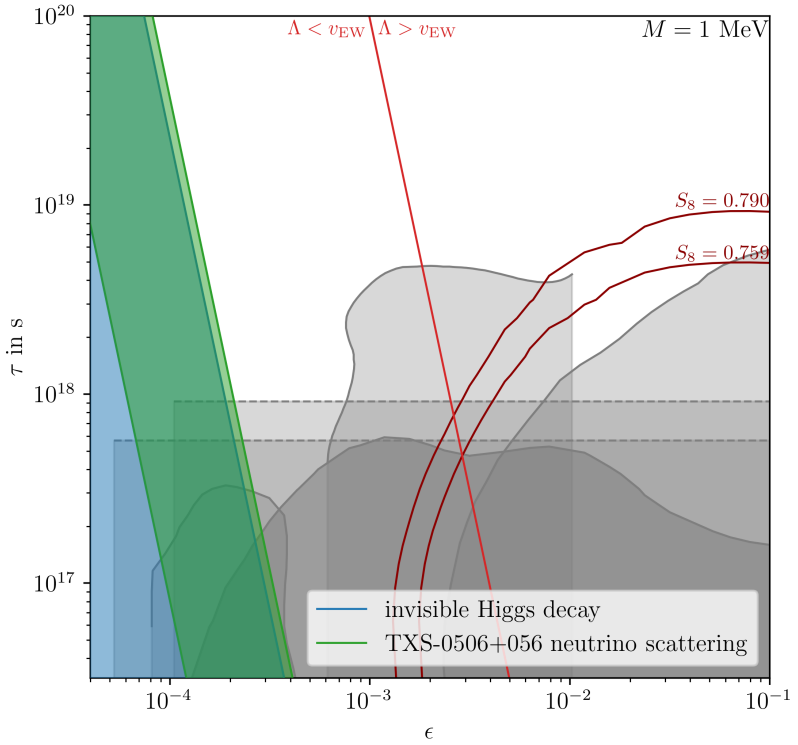

Figure 11. Exclusion plot for $M = 1\,\mathrm{MeV}$ showing the cosmological constraints in gray, the constraint from the invisible Higgs decay in blue and the IceCube constraint from high-energy neutrino scattering in green. The red line shows when Λ becomes smaller than v_{EW}.

JCAP01(2025)055

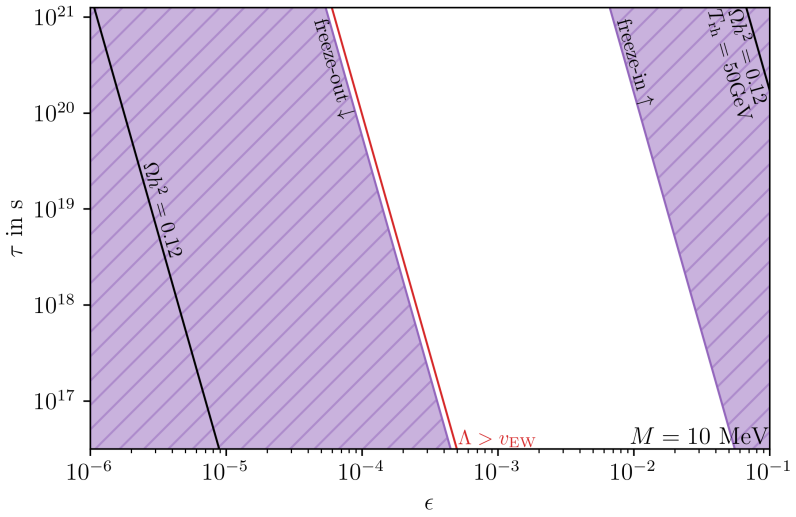

Figure 12. Regimes where production can occur via freeze-out (on the left side) as well as freeze-in (on the right) for an exemplary reheating temperature of $T_{\rm rh} = 50\,\text{GeV}$. In both cases, the black line indicates where a relic abundance of $\Omega h^2 = 0.12$ can be reached.

invisible Higgs decay is given by the scale of the Higgs mass which is comparable to $v_{\rm EW}$, the bound is clearly already in the regime where the EFT is non-sufficient. Thus, a UV completion would be required to assess constraints from invisible Higgs decay within the low-mass regime.

Lastly, the production mechanism explained in section 5 is also affected by the lowered mass because freeze-in requires a sufficiently weak coupling. Otherwise, the DM particles thermalize, and freeze-out occurs instead which happens for relevant values of ϵ and τ for lower masses of $M \simeq 10\,\text{MeV}$. To quantify this regime, we require that the production rate at a temperature equal to the DM mass has to be larger than the Hubble parameter $n_\nu \langle \sigma v \rangle (T = M)|_{\text{freeze-out}} > H(T = M)$. For the freeze-in regime, we conservatively require that the production rate at the reheating temperature is smaller than the Hubble rate $n_\nu \langle \sigma v \rangle (T = T_{\rm rh})|_{\text{freeze-in}} < H(T = T_{\rm rh})$, so that the back-reaction can always be neglected. In figure 12, both the freeze-in regime for an exemplary choice $T_{\rm rh} = 50\,\text{GeV}$ and the freeze-out regime are shown, for $M = 10\,\text{MeV}$. Solving the Boltzmann equation for freeze-out to determine the relic abundance of DM, results in the black line on the left, while the one on the right accounts for the freeze-in solution for the selected reheating temperature. We note that the freeze-out region corresponds to $\Lambda < v_{\rm EW}$, while all energy scales relevant for freeze-out are well below Λ. Nevertheless, a complete study of the phenomenology within the low-mass regime requires a UV completion, which is left to future work.

References

[1] N. Schöneberg et al., *The H0 Olympics: A fair ranking of proposed models*, *Phys. Rept.* **984** (2022) 1 [arXiv:2107.10291] [INSPIRE].

[2] PLANCK collaboration, *Planck 2018 results. VI. Cosmological parameters*, *Astron. Astrophys.* **641** (2020) A6 [*Erratum ibid.* **652** (2021) C4] [arXiv:1807.06209] [INSPIRE].

JCAP01(2025)055

[3] E. Abdalla et al., *Cosmology intertwined: A review of the particle physics, astrophysics, and cosmology associated with the cosmological tensions and anomalies*, *JHEAp* **34** (2022) 49 [arXiv:2203.06142] [INSPIRE].

[4] E. Di Valentino et al., *Cosmology Intertwined III: $f\sigma_8$ and S_8*, *Astropart. Phys.* **131** (2021) 102604 [arXiv:2008.11285] [INSPIRE].

[5] KiDS collaboration, *KiDS-1000 Cosmology: Cosmic shear constraints and comparison between two point statistics*, *Astron. Astrophys.* **645** (2021) A104 [arXiv:2007.15633] [INSPIRE].

[6] DES collaboration, *Dark Energy Survey Year 3 results: Cosmological constraints from galaxy clustering and weak lensing*, *Phys. Rev. D* **105** (2022) 023520 [arXiv:2105.13549] [INSPIRE].

[7] Kilo-Degree Survey and DES collaborations, *DES Y3 + KiDS-1000: Consistent cosmology combining cosmic shear surveys*, *Open J. Astrophys.* **6** (2023) 2305.17173 [arXiv:2305.17173] [INSPIRE].

[8] SPT and DES collaborations, *SPT clusters with DES and HST weak lensing. II. Cosmological constraints from the abundance of massive halos*, *Phys. Rev. D* **110** (2024) 083510 [arXiv:2401.02075] [INSPIRE].

[9] V. Ghirardini et al., *The SRG/eROSITA all-sky survey — Cosmology constraints from cluster abundances in the western Galactic hemisphere*, *Astron. Astrophys.* **689** (2024) A298 [arXiv:2402.08458] [INSPIRE].

[10] DESI collaboration, *DESI 2024 VII: Cosmological Constraints from the Full-Shape Modeling of Clustering Measurements*, arXiv:2411.12022 [INSPIRE].

[11] A. Amon and G. Efstathiou, *A non-linear solution to the S_8 tension?*, *Mon. Not. Roy. Astron. Soc.* **516** (2022) 5355 [arXiv:2206.11794] [INSPIRE].

[12] C. Preston, A. Amon and G. Efstathiou, *A non-linear solution to the S8 tension — II. Analysis of DES Year 3 cosmic shear*, *Mon. Not. Roy. Astron. Soc.* **525** (2023) 5554 [arXiv:2305.09827] [INSPIRE].

[13] Euclid collaboration, *Euclid preparation. I. The Euclid Wide Survey*, *Astron. Astrophys.* **662** (2022) A112 [arXiv:2108.01201] [INSPIRE].

[14] DESI collaboration, *The DESI Experiment Part I: Science,Targeting, and Survey Design*, arXiv:1611.00036 [INSPIRE].

[15] LSST collaboration, *LSST: from Science Drivers to Reference Design and Anticipated Data Products*, *Astrophys. J.* **873** (2019) 111 [arXiv:0805.2366] [INSPIRE].

[16] B. Audren et al., *Strongest model-independent bound on the lifetime of Dark Matter*, *JCAP* **12** (2014) 028 [arXiv:1407.2418] [INSPIRE].

[17] K. Enqvist, S. Nadathur, T. Sekiguchi and T. Takahashi, *Decaying dark matter and the tension in σ_8*, *JCAP* **09** (2015) 067 [arXiv:1505.05511] [INSPIRE].

[18] V. Poulin, P.D. Serpico and J. Lesgourgues, *A fresh look at linear cosmological constraints on a decaying dark matter component*, *JCAP* **08** (2016) 036 [arXiv:1606.02073] [INSPIRE].

[19] K. Enqvist, S. Nadathur, T. Sekiguchi and T. Takahashi, *Constraints on decaying dark matter from weak lensing and cluster counts*, *JCAP* **04** (2020) 015 [arXiv:1906.09112] [INSPIRE].

[20] A. Nygaard, T. Tram and S. Hannestad, *Updated constraints on decaying cold dark matter*, *JCAP* **05** (2021) 017 [arXiv:2011.01632] [INSPIRE].

[21] S. Alvi et al., *Do you smell something decaying? Updated linear constraints on decaying dark matter scenarios*, *JCAP* **11** (2022) 015 [arXiv:2205.05636] [INSPIRE].

JCAP01(2025)055

[22] Z. Berezhiani, A.D. Dolgov and I.I. Tkachev, *Reconciling Planck results with low redshift astronomical measurements*, *Phys. Rev. D* **92** (2015) 061303 [arXiv:1505.03644] [INSPIRE].

[23] T. Bringmann, F. Kahlhoefer, K. Schmidt-Hoberg and P. Walia, *Converting nonrelativistic dark matter to radiation*, *Phys. Rev. D* **98** (2018) 023543 [arXiv:1803.03644] [INSPIRE].

[24] K.L. Pandey, T. Karwal and S. Das, *Alleviating the H_0 and σ_8 anomalies with a decaying dark matter model*, *JCAP* **07** (2020) 026 [arXiv:1902.10636] [INSPIRE].

[25] DES collaboration, *Constraints on dark matter to dark radiation conversion in the late universe with DES-Y1 and external data*, *Phys. Rev. D* **103** (2021) 123528 [arXiv:2011.04606] [INSPIRE].

[26] A.H.G. Peter and A.J. Benson, *Dark-matter decays and Milky Way satellite galaxies*, *Phys. Rev. D* **82** (2010) 123521 [arXiv:1009.1912] [INSPIRE].

[27] S. Aoyama, K. Ichiki, D. Nitta and N. Sugiyama, *Formulation and constraints on decaying dark matter with finite mass daughter particles*, *JCAP* **09** (2011) 025 [arXiv:1106.1984] [INSPIRE].

[28] M.-Y. Wang and A.R. Zentner, *Effects of Unstable Dark Matter on Large-Scale Structure and Constraints from Future Surveys*, *Phys. Rev. D* **85** (2012) 043514 [arXiv:1201.2426] [INSPIRE].

[29] M.-Y. Wang et al., *Cosmological simulations of decaying dark matter: implications for small-scale structure of dark matter haloes*, *Mon. Not. Roy. Astron. Soc.* **445** (2014) 614 [arXiv:1406.0527] [INSPIRE].

[30] G. Blackadder and S.M. Koushiappas, *Dark matter with two- and many-body decays and supernovae type Ia*, *Phys. Rev. D* **90** (2014) 103527 [arXiv:1410.0683] [INSPIRE].

[31] S. Aoyama, T. Sekiguchi, K. Ichiki and N. Sugiyama, *Evolution of perturbations and cosmological constraints in decaying dark matter models with arbitrary decay mass products*, *JCAP* **07** (2014) 021 [arXiv:1402.2972] [INSPIRE].

[32] G. Blackadder and S.M. Koushiappas, *Cosmological constraints to dark matter with two- and many-body decays*, *Phys. Rev. D* **93** (2016) 023510 [arXiv:1510.06026] [INSPIRE].

[33] K. Vattis, S.M. Koushiappas and A. Loeb, *Dark matter decaying in the late Universe can relieve the H0 tension*, *Phys. Rev. D* **99** (2019) 121302 [arXiv:1903.06220] [INSPIRE].

[34] S.J. Clark, K. Vattis and S.M. Koushiappas, *Cosmological constraints on late-universe decaying dark matter as a solution to the H_0 tension*, *Phys. Rev. D* **103** (2021) 043014 [arXiv:2006.03678] [INSPIRE].

[35] B.S. Haridasu and M. Viel, *Late-time decaying dark matter: constraints and implications for the H_0-tension*, *Mon. Not. Roy. Astron. Soc.* **497** (2020) 1757 [arXiv:2004.07709] [INSPIRE].

[36] G. Franco Abellán, R. Murgia, V. Poulin and J. Lavalle, *Implications of the S_8 tension for decaying dark matter with warm decay products*, *Phys. Rev. D* **105** (2022) 063525 [arXiv:2008.09615] [INSPIRE].

[37] G. Franco Abellán, R. Murgia and V. Poulin, *Linear cosmological constraints on two-body decaying dark matter scenarios and the S8 tension*, *Phys. Rev. D* **104** (2021) 123533 [arXiv:2102.12498] [INSPIRE].

[38] Z. Davari and N. Khosravi, *Can decaying dark matter scenarios alleviate both H0 and $\sigma 8$ tensions?*, *Mon. Not. Roy. Astron. Soc.* **516** (2022) 4373 [arXiv:2203.09439] [INSPIRE].

[39] T. Simon et al., *Constraining decaying dark matter with BOSS data and the effective field theory of large-scale structures*, *Phys. Rev. D* **106** (2022) 023516 [arXiv:2203.07440] [INSPIRE].

JCAP01(2025)055

[40] L. Fuß and M. Garny, *Decaying Dark Matter and Lyman-α forest constraints*, *JCAP* **10** (2023) 020 [arXiv:2210.06117] [INSPIRE].

[41] E.B. Holm et al., *Decaying dark matter with profile likelihoods*, *Phys. Rev. D* **107** (2023) L021303 [arXiv:2211.01935] [INSPIRE].

[42] J. Bucko, S.K. Giri, F.H. Peters and A. Schneider, *Probing the two-body decaying dark matter scenario with weak lensing and the cosmic microwave background*, *Astron. Astrophys.* **683** (2024) A152 [arXiv:2307.03222] [INSPIRE].

[43] N.F. Bell, A.J. Galea and K. Petraki, *Lifetime Constraints for Late Dark Matter Decay*, *Phys. Rev. D* **82** (2010) 023514 [arXiv:1004.1008] [INSPIRE].

[44] N.F. Bell, A.J. Galea and R.R. Volkas, *A Model For Late Dark Matter Decay*, *Phys. Rev. D* **83** (2011) 063504 [arXiv:1012.0067] [INSPIRE].

[45] K. Hamaguchi, K. Nakayama and Y. Tang, *Gravitino/Axino as Decaying Dark Matter and Cosmological Tensions*, *Phys. Lett. B* **772** (2017) 415 [arXiv:1705.04521] [INSPIRE].

[46] K.J. Bae, A. Kamada and H.J. Kim, *Decaying axinolike dark matter: Discriminative solution to small-scale issues*, *Phys. Rev. D* **99** (2019) 023511 [arXiv:1806.08569] [INSPIRE].

[47] G. Choi and T.T. Yanagida, *Gravitino cosmology helped by a right handed (s)neutrino*, *Phys. Lett. B* **827** (2022) 136954 [arXiv:2104.02958] [INSPIRE].

[48] M. Deshpande, *A study of supersymmetric decaying dark matter models*, Ph.D. thesis, Adelaide University, Australia (2023) [INSPIRE].

[49] G. Obied, C. Dvorkin, E. Gonzalo and C. Vafa, *Dark dimension and decaying dark matter gravitons*, *Phys. Rev. D* **109** (2024) 063540 [arXiv:2311.05318] [INSPIRE].

[50] A. Cheek, J.K. Osiński, L. Roszkowski and S. Trojanowski, *Dark matter production through a non-thermal flavon portal*, *JHEP* **03** (2023) 149 [arXiv:2211.02057] [INSPIRE].

[51] DES collaboration, *Milky Way Satellite Census. IV. Constraints on Decaying Dark Matter from Observations of Milky Way Satellite Galaxies*, *Astrophys. J.* **932** (2022) 128 [arXiv:2201.11740] [INSPIRE].

[52] A. Nygaard, E.B. Holm, T. Tram and S. Hannestad, *Decaying Dark Matter and the Hubble Tension*, arXiv:2307.00418 [INSPIRE].

[53] eBOSS collaboration, *The one-dimensional power spectrum from the SDSS DR14 Lyα forests*, *JCAP* **07** (2019) 017 [arXiv:1812.03554] [INSPIRE].

[54] J. Lesgourgues and T. Tram, *The Cosmic Linear Anisotropy Solving System (CLASS) IV: efficient implementation of non-cold relics*, *JCAP* **09** (2011) 032 [arXiv:1104.2935] [INSPIRE].

[55] M. Garny, A. Ibarra, D. Tran and C. Weniger, *Gamma-Ray Lines from Radiative Dark Matter Decay*, *JCAP* **01** (2011) 032 [arXiv:1011.3786] [INSPIRE].

[56] J. Berteaud et al., *Strong constraints on primordial black hole dark matter from 16 years of INTEGRAL/SPI observations*, *Phys. Rev. D* **106** (2022) 023030 [arXiv:2202.07483] [INSPIRE].

[57] F. Calore, A. Dekker, P.D. Serpico and T. Siegert, *Constraints on light decaying dark matter candidates from 16 yr of INTEGRAL/SPI observations*, *Mon. Not. Roy. Astron. Soc.* **520** (2023) 4167 [arXiv:2209.06299] [INSPIRE].

[58] R. Essig et al., *Constraining Light Dark Matter with Diffuse X-Ray and Gamma-Ray Observations*, *JHEP* **11** (2013) 193 [arXiv:1309.4091] [INSPIRE].

JCAP01(2025)055

[59] P. De la Torre Luque, S. Balaji and J. Koechler, *Importance of Cosmic-Ray Propagation on Sub-GeV Dark Matter Constraints*, *Astrophys. J.* **968** (2024) 46 [arXiv:2311.04979] [INSPIRE].

[60] P. De la Torre Luque, S. Balaji and J. Silk, *New 511 keV Line Data Provide Strongest sub-GeV Dark Matter Constraints*, *Astrophys. J. Lett.* **973** (2024) L6 [arXiv:2312.04907] [INSPIRE].

[61] H.-B. Jin, Y.-L. Wu and Y.-F. Zhou, *Implications of the first AMS-02 measurement for dark matter annihilation and decay*, *JCAP* **11** (2013) 026 [arXiv:1304.1997] [INSPIRE].

[62] C.A. Argüelles et al., *Dark matter decay to neutrinos*, *Phys. Rev. D* **108** (2023) 123021 [arXiv:2210.01303] [INSPIRE].

[63] BOREXINO collaboration, *Search for low-energy neutrinos from astrophysical sources with Borexino*, *Astropart. Phys.* **125** (2021) 102509 [arXiv:1909.02422] [INSPIRE].

[64] KAMLAND collaboration, *Limits on Astrophysical Antineutrinos with the KamLAND Experiment*, *Astrophys. J.* **925** (2022) 14 [arXiv:2108.08527] [INSPIRE].

[65] SUPER-KAMIOKANDE collaboration, *Diffuse supernova neutrino background search at Super-Kamiokande*, *Phys. Rev. D* **104** (2021) 122002 [arXiv:2109.11174] [INSPIRE].

[66] A. Olivares-Del Campo, C. Bœhm, S. Palomares-Ruiz and S. Pascoli, *Dark matter-neutrino interactions through the lens of their cosmological implications*, *Phys. Rev. D* **97** (2018) 075039 [arXiv:1711.05283] [INSPIRE].

[67] JUNO collaboration, *Physics potential with astrophysical neutrinos in JUNO*, *PoS* **ICRC2023** (2023) 1192 [INSPIRE].

[68] K. Akita, G. Lambiase, M. Niibo and M. Yamaguchi, *Neutrino lines from MeV dark matter annihilation and decay in JUNO*, *JCAP* **10** (2022) 097 [arXiv:2206.06755] [INSPIRE].

[69] DUNE collaboration, *Deep Underground Neutrino Experiment (DUNE), Far Detector Technical Design Report, Volume II: DUNE Physics*, arXiv:2002.03005 [INSPIRE].

[70] C.A. Argüelles et al., *Dark matter annihilation to neutrinos*, *Rev. Mod. Phys.* **93** (2021) 035007 [arXiv:1912.09486] [INSPIRE].

[71] HYPER-KAMIOKANDE collaboration, *Hyper-Kamiokande detector and its capabilities in astrophysical neutrino search*, *J. Phys. Conf. Ser.* **2429** (2023) 012030 [INSPIRE].

[72] N.F. Bell, M.J. Dolan and S. Robles, *Searching for Sub-GeV Dark Matter in the Galactic Centre using Hyper-Kamiokande*, *JCAP* **09** (2020) 019 [arXiv:2005.01950] [INSPIRE].

[73] M. D'Onofrio and K. Rummukainen, *Standard model cross-over on the lattice*, *Phys. Rev. D* **93** (2016) 025003 [arXiv:1508.07161] [INSPIRE].

[74] L.J. Hall, K. Jedamzik, J. March-Russell and S.M. West, *Freeze-In Production of FIMP Dark Matter*, *JHEP* **03** (2010) 080 [arXiv:0911.1120] [INSPIRE].

[75] J. Edsjo and P. Gondolo, *Neutralino relic density including coannihilations*, *Phys. Rev. D* **56** (1997) 1879 [hep-ph/9704361] [INSPIRE].

[76] G.F. Giudice, E.W. Kolb and A. Riotto, *Largest temperature of the radiation era and its cosmological implications*, *Phys. Rev. D* **64** (2001) 023508 [hep-ph/0005123] [INSPIRE].

[77] G. Franco Abellán et al., *Fast likelihood-free inference in the LSS Stage IV era*, *JCAP* **11** (2024) 057 [arXiv:2403.14750] [INSPIRE].

[78] PARTICLE DATA GROUP collaboration, *Review of Particle Physics*, *PTEP* **2022** (2022) 083C01 [INSPIRE].

JCAP01(2025)055

[79] E. Di Valentino, C. Bøehm, E. Hivon and F.R. Bouchet, *Reducing the H_0 and σ_8 tensions with Dark Matter-neutrino interactions*, *Phys. Rev. D* **97** (2018) 043513 [arXiv:1710.02559] [INSPIRE].

[80] P. Brax et al., *Extended analysis of neutrino-dark matter interactions with small-scale CMB experiments*, *Phys. Dark Univ.* **42** (2023) 101321 [arXiv:2305.01383] [INSPIRE].

[81] W. Giarè, A. Gómez-Valent, E. Di Valentino and C. van de Bruck, *Hints of neutrino dark matter scattering in the CMB? Constraints from the marginalized and profile distributions*, *Phys. Rev. D* **109** (2024) 063516 [arXiv:2311.09116] [INSPIRE].

[82] R.J. Wilkinson, C. Bøehm and J. Lesgourgues, *Constraining Dark Matter-Neutrino Interactions using the CMB and Large-Scale Structure*, *JCAP* **05** (2014) 011 [arXiv:1401.7597] [INSPIRE].

[83] J.A.D. Diacoumis and Y.Y.Y. Wong, *On the prior dependence of cosmological constraints on some dark matter interactions*, *JCAP* **05** (2019) 025 [arXiv:1811.11408] [INSPIRE].

[84] M.R. Mosbech et al., *The full Boltzmann hierarchy for dark matter-massive neutrino interactions*, *JCAP* **03** (2021) 066 [arXiv:2011.04206] [INSPIRE].

[85] M. Escudero et al., *Exploring dark matter microphysics with galaxy surveys*, *JCAP* **09** (2015) 034 [arXiv:1505.06735] [INSPIRE].

[86] D.C. Hooper and M. Lucca, *Hints of dark matter-neutrino interactions in Lyman-α data*, *Phys. Rev. D* **105** (2022) 103504 [arXiv:2110.04024] [INSPIRE].

[87] K. Akita and S. Ando, *Constraints on dark matter-neutrino scattering from the Milky-Way satellites and subhalo modeling for dark acoustic oscillations*, *JCAP* **11** (2023) 037 [arXiv:2305.01913] [INSPIRE].

[88] G. Mangano et al., *Cosmological bounds on dark matter-neutrino interactions*, *Phys. Rev. D* **74** (2006) 043517 [astro-ph/0606190] [INSPIRE].

[89] R. Diamanti et al., *Dark Radiation and interacting scenarios*, *Phys. Rev. D* **87** (2013) 063509 [arXiv:1212.6007] [INSPIRE].

[90] IceCube collaboration, *Neutrino emission from the direction of the blazar TXS 0506+056 prior to the IceCube-170922A alert*, *Science* **361** (2018) 147 [arXiv:1807.08794] [INSPIRE].

[91] Y.T. Tanaka, S. Buson and D. Kocevski, *Fermi-LAT detection of increased gamma-ray activity of TXS 0506+056, located inside the IceCube-170922A error region*, *The Astronomer's Telegram* **10791** (2017) 1.

[92] K.-Y. Choi, J. Kim and C. Rott, *Constraining dark matter-neutrino interactions with IceCube-170922A*, *Phys. Rev. D* **99** (2019) 083018 [arXiv:1903.03302] [INSPIRE].

[93] F. Ferrer, G. Herrera and A. Ibarra, *New constraints on the dark matter-neutrino and dark matter-photon scattering cross sections from TXS 0506+056*, *JCAP* **05** (2023) 057 [arXiv:2209.06339] [INSPIRE].

[94] J.M. Cline and M. Puel, *NGC 1068 constraints on neutrino-dark matter scattering*, *JCAP* **06** (2023) 004 [arXiv:2301.08756] [INSPIRE].

[95] G. Raffelt, *Stars as Laboratories for Fundamental Physics — The Astrophysics of Neutrinos, Axions, and Other Weakly Interacting Particles*, University of Chicago Press (1996).

[96] S. Heston, S. Horiuchi and S. Shirai, *Constraining neutrino-DM interactions with Milky Way dwarf spheroidals and supernova neutrinos*, *Phys. Rev. D* **110** (2024) 023004 [arXiv:2402.08718] [INSPIRE].

JCAP01(2025)055

[97] V. Shtabovenko, R. Mertig and F. Orellana, *FeynCalc 9.3: New features and improvements*, *Comput. Phys. Commun.* **256** (2020) 107478 [arXiv:2001.04407] [INSPIRE].

[98] J.R. Ellis, M.K. Gaillard and D.V. Nanopoulos, *A Phenomenological Profile of the Higgs Boson*, *Nucl. Phys. B* **106** (1976) 292 [INSPIRE].

[99] R. Gastmans, S.L. Wu and T.T. Wu, *Higgs Decay into Two Photons, Revisited*, arXiv:1108.5872 [INSPIRE].

[100] D. Huang, Y. Tang and Y.-L. Wu, *Note on Higgs Decay into Two Photons $H \to \gamma\gamma$*, *Commun. Theor. Phys.* **57** (2012) 427 [arXiv:1109.4846] [INSPIRE].

[101] W.J. Marciano, C. Zhang and S. Willenbrock, *Higgs Decay to Two Photons*, *Phys. Rev. D* **85** (2012) 013002 [arXiv:1109.5304] [INSPIRE].

[102] J. Davies and F. Herren, *Higgs boson decay into photons at four loops*, *Phys. Rev. D* **104** (2021) 053010 [arXiv:2104.12780] [INSPIRE].

JCAP01(2025)055